HHS Public Access

Author manuscript

Neuron. Author manuscript; available in PMC 2023 September 21.

Published in final edited form as:

Neuron. 2022 September 21; 110(18): 3000–3017.e8. doi:10.1016/j.neuron.2022.06.026.

VMHvll^{Cckar} Cells Dynamically Control Female Sexual Behaviors over Reproductive Cycle

Luping Yin[1,*], **Koichi Hashikawa**[1], **Yoshiko Hashikawa**[1], **Takuya Osakada**[1], **Julieta E. Lischinsky**[1], **Veronica Diaz**[1], **Dayu Lin**[1,2,3,*]

[1]Neuroscience Institute, New York University Langone Medical Center, New York, NY 10016, USA

[2]Department of Psychiatry, New York University Langone Medical Center, New York, NY

[3]Lead contact

Summary

Sexual behavior is fundamental for the survival of mammalian species and thus supported by dedicated neural substrates. The ventrolateral part of ventromedial hypothalamus (VMHvl) is an essential locus for controlling female sexual behaviors, but recent studies revealed molecular complexity and functional heterogeneity of VMHvl cells. Here, we identify the cholecystokinin A receptor (Cckar) expressing cells in the lateral VMHvl (VMHvll^{Cckar}) as key controllers for female sexual behaviors. Inactivation of VMHvll^{Cckar} cells in female mice diminishes their interest of males and sexual receptivity while activating these cells has the opposite effects. Female sexual behaviors vary drastically over reproductive cycle. *In vivo* recordings reveal reproductive-state dependent changes of VMHvll^{Cckar} cell spontaneous activity and responsivity, with the highest activity during estrus. These *in vivo* response changes coincide with robust alternation in VMHvll^{Cckar} cell excitability and synaptic inputs. Altogether, VMHvll^{Cckar} cells represent a key neural population dynamically controlling female sexual behaviors over reproductive cycle.

eTOC blurb

Yin et al. establish VMHvll^{Cckar} cells as a hub orchestrating female sexual behaviors and a brake for female aggression. VMHvll^{Cckar} cells undergo dramatic cellular and synaptic changes over reproductive cycle to alter the cell responsivity to male cues and control timing of female sexual behaviors.

[*]Correspondences: luping.yin@nyulangone.org and dayu.lin@nyulangone.org.

Author Contributions

D.L conceived and supervised the project, designed experiments, analyzed the data and wrote the manuscript. L.Y. designed experiments, conducted nearly all experiments, analyzed the data and co-wrote the manuscript. K.H., and Y.H. generated the Cckar^{Cre} transgenic mouse line. T.O. performed in situ hybridization. J.L., and V.D. performed initial characterization of the Cckar^{Cre} transgenic line and conducted pilot chemogenetic activation experiment.

Declaration of Interests

The authors declare no competing interests.

Graphical Abstract

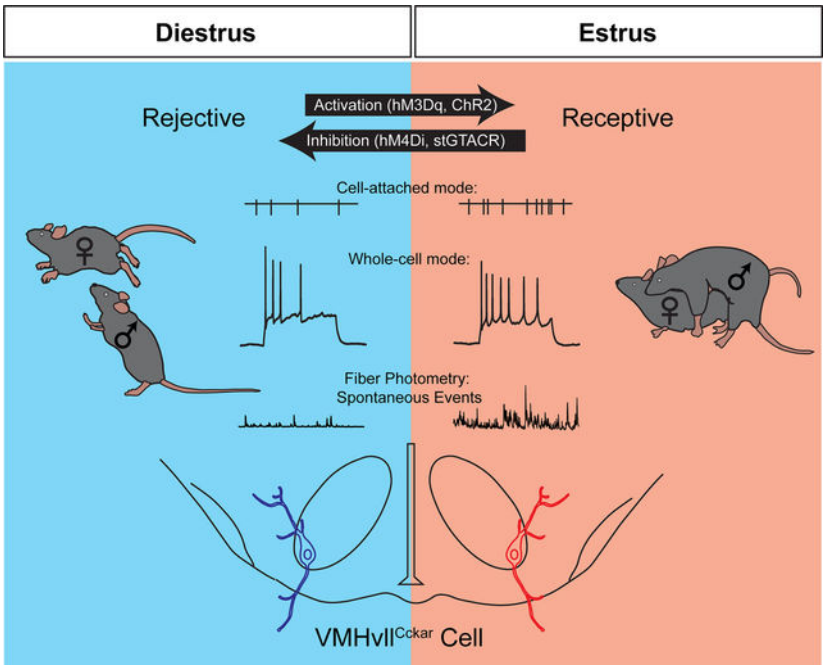

Keywords

Female sexual behavior; maternal aggression; ventrolateral part of ventromedial hypothalamus; cholecystokinin A receptor; neural plasticity; reproductive cycle

Introduction

Sexual behavior is of paramount importance for the survival and propagation of mammalian species. Three concepts have been proposed to characterize female sexual behaviors: attractivity, proceptivity, and receptivity (Beach, 1976; Micevych and Meisel, 2017). “Attractivity” refers to the stimulus value of the female in evoking interest and sexual behaviors from the male. “Proceptivity” refers to various behaviors initiated by the females, e.g. approach, that could lead to sexual interaction. “Receptivity” describes the tendency of a female in allowing interactions initiated by the male that ultimately results in intravaginal ejaculation and fertilization (Beach, 1976).

To maximize the reproduction success while minimizing energy-consuming non-productive copulation, all three aspects of female’s sexual behaviors are intimately coupled to the female’s reproductive cycle, including estrous cycle during virgin state as well as lactation (Beach, 1976; Inoue, 2021; Jennings and de Lecea, 2020). In rodents, estrous females show increased preference to male cues, i.e. higher proceptivity, and higher sexual receptivity during the period surrounding ovulation, i.e. estrus (Dey et al., 2015; Eliasson and Meyerson, 1975; Hardy, 1972; McCarthy et al., 2018). As to attractivity, sexually experienced males are more attracted to estrous than diestrous females (Hayashi and Kimura, 1974; Kavaliers et al., 1994). During lactation, female sexual behaviors are

strongly suppressed. Instead, lactating females attack male intruders to protect their young, a phenomenon known as maternal aggression (Gandelman, 1972; Green, 1978). While sex hormones have been implicated in the behavior change over reproductive cycle, the underlying cellular and circuit mechanisms remain incompletely understood (Jennings and de Lecea, 2020).

The ventrolateral part of the ventromedial hypothalamus (VMHvl) is essential for female sexual behaviors (Lenschow and Lima, 2020; Micevych and Meisel, 2017). Lesioning the VMHvl disrupts female sexual receptivity in many species (Goy and Phoenix, 1963; Kendrick et al., 1995; Leedy and Hart, 1985; Mathews et al., 1983; Robarts and Baum, 2007). Recent studies in rodents identified the VMHvl cells that express estrogen receptor alpha ($VMHvl^{Esr1}$), which mostly also express progesterone receptor (PR), as an important population for female sexual behaviors (Inoue et al., 2019; Musatov et al., 2006; Yang et al., 2013). Inactivation of $VMHvl^{Esr1}$ cells or knocking down Esr1 in the VMHvl decreases female sexual receptivity (Inoue et al., 2019; Musatov et al., 2006; Yang et al., 2013). Surprisingly, activating $VMHvl^{Esr1}$ cells failed to increase female sexual receptivity in mice (Hashikawa et al., 2017a; Yang et al., 2013). This negative gain-of-function result may be due to the molecular and functional heterogeneity of $VMHvl^{Esr1}$ cells. Indeed, our Fos mapping and RNA sequencing revealed two molecularly distinct compartments in the female VMHvl (Hashikawa et al., 2017a). Female aggression-induced Fos mainly occupies the medial compartment (VMHvlm) while mating-induced Fos is concentrated in the lateral compartment (VMHvll)(Hashikawa et al., 2017a). More detailed single cell RNA sequencing (scRNAseq) further confirmed the high molecular diversity of $VMHvl^{Esr1}$ cells (Kim et al., 2019; Knoedler et al., 2022). Most recently, Liu et. al. identified Npy2r expressing VMHvl cells ($VMHvl^{Npy2r}$) as the female aggression relevant population. When $VMHvl^{Esr1+}$cells that do not express Npy2r ($VMHvl^{Esr1+Npy2r-}$) were optogenetically activated, female sexual receptivity could indeed be enhanced (Liu et al., 2022). However, $VMHvl^{Esr1+Npy2r-}$ cells cover approximately 70% of all $VMHvl^{Esr1}$ cells and are composed of multiple molecularly distinct subpopulations, most of which are not activated by female sexual behaviors (Liu et al., 2022).

The morphology of VMHvl cells changes dramatically over the reproductive cycle (Inoue et al., 2019; Madeira et al., 2001). *In vivo* single unit recordings also revealed changes in VMHvl cell responses to male cues over estrous cycle (Hashikawa et al., 2017a; Nomoto and Lima, 2015). However, bulk Ca^{2+} recordings of $VMHvl^{Esr1}$, $VMHvl^{PR}$ or $VMHvl^{Esr1+Npy2r-}$ cells failed to reveal changes in responses to social stimuli over reproductive cycle (Hashikawa et al., 2017a; Inoue et al., 2019; Liu et al., 2022). Instead, the axon terminals of $VMHvl^{Esr1}$ cells (Kim et al., 2019) and the aggression related $VMHvl^{Esr1}$ cells were found to experience reproductive state dependent variations (Liu et al., 2022). Thus, the current model puts the VMHvl aggression cells as the primary driving force for the behavioral switch from virgin to lactation (Liu et al., 2022), while the main contribution of reproduction-related cells is to alter synaptic output during estrous cycle (Kim et al., 2019). However, given that both $VMHvl^{Esr1}$ and $VMHvl^{Esr1+Npy2r-}$ cells contain a large percentage of reproduction-unrelated cells, changes of VMHvl reproduction cells could be masked by reproduction-unrelated cells.

Here, following up on our previous RNAseq results at the VMHvl (Hashikawa et al., 2017a), we investigated the role of VMHvl cells that express cholecystokinin A receptor (Cckar), a gene concentrated in the VMHvll (Hashikawa et al., 2017a). Using a newly generated $Cckar^{Cre}$ mouse line, we demonstrated the functional importance of Cckar expressing VMHvll cells ($VMHvll^{Cckar}$) in controlling multiple aspects of female sexual behaviors and revealed dramatic changes of their *in vivo* activity and electrophysiological properties over reproductive cycle.

Results

Characterization of $VMHvll^{Cckar}$ cells

To target Cckar expressing cells, we generated a $Cckar^{Cre}$ knock-in mouse line (Figure S1). Double *in situ* hybridization revealed over 90% overlap between *Cre* and *Cckar* mRNA (Figures 1A–1B). Consistent with the sexually dimorphic expression of *Cckar* (Xu et al., 2012), after crossing the $Cckar^{Cre}$ line with a ZsGreen reporter line (Ai6) (Madisen et al., 2010), we observed significantly more ZsGreen expressing cells in the female VMHvl than the male (Figures S2A–S2C). In addition, Cckar expression is strongly biased to the VMHvll in females but not males (Figure S2D). Virtually all Cckar+ cells express Esr1 (94%), whereas approximately 50% of Esr1+ cells express Cckar (Figures 1C–1D). The extent of overlap is significantly higher than the chance level as Esr1 and Cckar are expressed in 74% and 37% of total VMHvll cells, respectively (Figures 1C, 1D and 1I). Furthermore, we observed a preferential overlap between Fos and Cckar after female sexual behaviors (Figures 1E–1F). Consistent with our previous findings (Hashikawa et al., 2017a), mating induced Fos was largely confined in the VMHvll in females (Figure S2F). Within the VMHvll, approximately 70% of Fos cells express Cckar whereas over 60% of Cckar cells express Fos, both significantly higher than the chance level (~40%) (Figures 1E, 1F and 1I). We further examined the relationship between $VMHvll^{Cckar}$ and the recently identified female VMHvl aggression- ($VMHvl^{Npy2r}$) and reproduction-related ($VMHvl^{Esr1+Npy2r-}$) cells (Liu et al., 2022) (Figure S2G). Triple *in situ* hybridization of *Esr1, Cckar,* and *Npy2r*, revealed that Nyp2r and Cckar occupy largely spatially distinct regions within the VMHvl and overlap minimally (Figures S2G–S2J). The distribution of $VMHvl^{Esr1+Npy2r-}$ cells is VMHvll-biased but to a much lesser extent in comparison to Cckar+ cells (Figure S2H). Approximately one third (35%) of Esr1+Npy2r− cells express Cckar, while most Cckar+ cells (82%) are Esr1+Npy2r−, suggesting that Cckar+ cells are a more limited VMHvl subpopulation in comparison to Esr1+Npy2r− cells (Figures S2I–S2J).

We found previously that VMHvll cells, in comparison to VMHvlm cells, project preferentially to anteroventral periventricular nucleus (AVPV), a region enriched of kisspeptin, an important neuropeptide for female sexual behaviors (Hashikawa et al., 2017a; Hellier et al., 2019). To understand whether Cckar+ cells represent the main source of VMHvl input to AVPV, we injected retrobeads into the AVPV and, as expected, observed laterally biased labeling within the VMHvl (Figures S3A–S3B). Within the VMHvll, nearly 70% of Cckar+ cells are labeled with retrobeads whereas over 85% of all retrobead-labeled cells express Cckar, suggesting Cckar+ cells as the primary input to AVPV originating from the VMHvl (Figures 1G–1H). Consistent with the retrograde labeling results, anterograde

tracing from the VMHvll^{Cckar} cells revealed AVPV as the region containing the densest axon terminals (Figures 1J–1M). Beyond AVPV, VMHvll^{Cckar} cells mainly target regions within the hypothalamus, including medial preoptic area (mPOA), tuberal nucleus (Tu), arcuate nucleus (ARC) and dorsal medial hypothalamus (DMH) among others (Figures 1M and S3D–S3E). Outside of the hypothalamus, moderate fibers were found in the posterior amygdala (PA), medial amygdala (MeA), bed nucleus of stria terminalis (BNST), paraventricular nucleus of the thalamus (PVT) and several midbrain regions, including the mesencephalic reticular formation (mRt)—a region relevant for lordosis reflex (Gorski, 1976) (Figures S3C–S3E). Together, these results suggest that Cckar+ cells are potentially the VMHvll subpopulation preferentially relevant for female sexual behaviors.

Characterizing female sexual behaviors during various reproductive states

We first sought to gain a comprehensive understanding of female sexual behaviors across reproductive states. We introduced a highly sexually experienced male mouse into the home cage of singly housed female mice at different reproductive states and characterized their behaviors in 94 pairs of animals (Figure S4). All males approached and tried to mount the female repeatedly regardless of the female's reproductive state likely due to their extensive sexual experience (Figures S4A–S4H). In contrast, female behaviors varied significantly with their reproductive state (Figures S4A–S4E, S4I–S4J). Diestrous and non-aggressive lactating females actively rejected male's mounting attempt by staying upright, pushing and darting away (Figures S4D–S4E, and S4K), rarely approached the male (Figure S4L) and never lordosed when the male forced mount (Figure S4M). As a result, males had a low success in establishing mounting (Figure S4N) and never achieved intromission (Figure S4O).

Consistent with the fact that vaginal estrus and behavior estrus do not always match (Le Moene et al., 2020), we observed more behavior variability in estrous females and separated them into three groups based on lordosis quotient (LQ): non-receptive (LQ=0), semi-receptive (LQ<50%), and fully receptive (LQ>50%) (Figures S4A–S4C). The non-receptive estrous female behaved similarly to diestrous females, showing high rejection and low approach frequency (Figures S4K–S4L). In contrast, fully receptive females approached the male frequently, showed little rejection, and consequently males always succeeded in establishing a mounting position and advancing to intromission in approximately 2/3 of mounting trials (Figures S4K–S4O). Semi-receptive females behaved in between (Figures S4I–S4O). Although the males were able to achieve intromission in approximately half of the mounting trials, semi-receptive females were not fully cooperative, spending most of their time wiggling instead of lordosing when being mounted by the male (Figures S4I, S4J and S4O). When all behaviors were considered together, the total interaction time (TIT) in fully receptive females was longer than that of non-receptive estrous and diestrous females, but did not differ significantly from semi-receptive estrus females and non-aggressive lactating females (Figure S4P).

Chemogenetic inhibition of VMHvll^{Cckar} cells suppresses female sexual behaviors

To address the functional role of VMHvll^{Cckar} cells in female sexual behaviors, we virally expressed hM4Di in female VMHvll^{Cckar} cells (Cckar^{hM4Di}) (Figure 2A) (Armbruster et al.,

2007). On each test day, the female was first paired with a sexually experienced adult male for ~10 minutes to determine its receptivity level, then injected with CNO or saline, and 30 minutes later tested again with a different sexually experienced male for ~10 minutes (Figure 2B).

In semi- or fully- receptive estrous females, CNO injection, in comparison to saline injection, significantly increased rejection against male's close investigation and mounting attempts (Figures 2C and 2D), decreased approach frequency (Figures 2C and 2E), and reduced LQ (Figures 2C and 2F). Accordingly, males had a lower mounting success rate and could not achieve intromission efficiently (Figures 2G–2H). The change in rejection and receptivity is not due to changes in locomotion. In solitary females, CNO injection did not change movement speed (Figure 2I).

We further examined the effect of VMHvll^{Cckar} inactivation in female's interest towards males using a three-chamber social preference test (Figure 2J)(Kaidanovich-Beilin et al., 2011). As expected, estrous females preferred an unfamiliar male over an unfamiliar diestrous female (Figures S5A–S5B), and CNO injection completely reversed such preference (Figure 2K). However, inactivating VMHvll^{Cckar} cells did not alter female's attractiveness. Although sexually experienced males showed a clear preference towards estrous females over diestrous females (Figures S5E–S5F), they spent similar amounts of time interacting with CNO-injected and saline-injected estrous Cckar^{hM4Di} females (Figures 2L–2M). In control estrous females that were injected with mCherry virus (Cckar^{mCherry}), we observed no change in sexual interest or receptivity after CNO injection (Figures 2D–2M). Likely due to the naturally low level of sexual receptivity in diestrous and lactating females, their behaviors towards males did not change after VMHvll^{Cckar} cell inactivation (Figure S6). Beyond sexual behaviors, we observed no change in behaviors during female-juvenile, female-female, and female-pup interactions, across all reproductive states except a decrease in pup grooming in estrous females (Figure S7).

Lastly, given the estrous cycle dependent body temperature change (Sanchez-Alavez et al., 2011), we examined the effect of VMHvll^{Cckar} cell inhibition on core body temperature using an implantable temperature logger (Figures S8A–S8B). CNO injection but not saline injection significantly decreased the average core body temperature in Cckar^{hM4Di} mice by clamping down the temperature fluctuation to the floor of its normal range while having no effect in Cckar^{mCherry} mice (Figures S8C–S8F).

Optogenetic inactivation of VMHvll^{Cckar} acutely reduces female sexual receptivity

Chemogenetic inhibition test occurs over a period of 30–60 minutes, which may be sufficient for hormonal changes. To understand whether VMHvll^{Cckar} cell activity could influence female sexual behavior within seconds, a time window that is unlikely to cause changes in circulating sex hormone levels, we optogenetically inactivated VMHvll^{Cckar} cells by expressing stGtACR2 in VMHvll^{Cckar} cells (Cckar^{stGtACR2}) (Mahn et al., 2018) (Figure 3A). The light and sham stimulation started when the male successfully mounted the test estrous female (Figure 3B). While the females showed stationary lordosis posture in sham trials, females wiggled and increased rejection upon light stimulation (Figure 3C). We calculated the female sexual behavior score (SBS) for each video frame and found that

while light had no effect on SBS in Cckar^{GFP} animals (Figure 3D), it suppressed SBS nearly instantaneously in Cckar^{stGtACR2} mice (Figure 3E). Due to the decreased sexual receptivity of Cckar^{stGtACR2} females, the male SBS also decreased quickly after light onset (Figure 3l). Across animals, optogenetic inhibition of VMHvll^{Cckar} cells significantly increased female's efforts to actively reject the male, decreased lordosis duration, male intromission success rate and intromission duration per trial (Figures 3F, 3G, 3J and 3K).

Chemogenetic activation of VMHvll^{Cckar} cells promotes female sexual behaviors and inhibits female aggression

To address whether activation of VMHvll^{Cckar} cells is sufficient to enhance female sexual behaviors, we virally expressed hM3Dq in VMHvll^{Cckar} cells (Cckar^{hM3Dq}) (Figures 4A–4B). After CNO but not saline injection, diestrous Cckar^{hM3Dq} female showed less rejection when the male investigated or attempted to mount (Figures 4C and 4D) and approached the male more frequently (Figures 4C–4E). Impressively, females changed from completely non-receptive to semi- or fully- receptive 30 min after CNO injection (Figures 4C and 4F). As a result, males succeeded in mounting in the vast majority of attempted trials and achieving intromission in approximately 60% of mounting trials whereas males were never able to intromit when paired with saline-injected Cckar^{hM3Dq} or CNO-injected Cckar^{mCherry} diestrous females (Figures 4G–4H). In the three chamber preference test, diestrous females normally spent more time interacting with a diestrous female over a male (Figures S5C–S5D). After CNO injection, diestrous Cckar^{hM3Dq} females, but not Cckar^{mCherry} females, preferred males over diestrous females (Figures 4I–4J) although the manipulation did not increase female's attractiveness to a sexually experienced male mouse (Figures 4K–4L). The increase in female sexual behaviors was also observed in non-receptive and semi-receptive estrous females after CNO injection (Figures S9A–S9D). However, activating VMHvll^{Cckar} cells in lactating females only slightly increased female sexual receptivity in a subset of animals (2/8), suggesting possible different neural mechanisms underlying reduced female receptivity during diestrus and lactation (Figure S9E–S9H).

We further asked whether VMHvll^{Cckar} activation-induced increase in female sexual behaviors is dependent on sex hormones by using ovariectomized (OVX) females (Figures 4M–4R). In comparison to saline injection, CNO injection significantly decreased rejection, increased approach frequency towards the male, and increased LQ of OVX Cckar^{hM3Dq} females (Figures 4N–4P). The paired male significantly increased mounting success rate but was not able to intromit likely due to the narrow vaginal opening in OVX females (Figures 4S–4T). These results suggest that VMHvll^{Cckar} activation could promote female sexual behaviors independent of the sex hormone actions.

VMHvll^{Cckar} activation also decreased female aggression towards juveniles in both virgin and lactating females, suggesting an inhibitory effect of VMHvll^{Cckar} cells onto the aggression circuit upon their activation (Figures S10C, S10F and S10l). Interaction with a female was not altered in virgin Cckar^{hM3Dq} females but was suppressed during lactation, possibly due to the aggression-motivated nature of the interaction (Figures S10D, S10G and S10J). CNO injection did not change pup-directed behaviors (Figures S10E, S10H and S10K).

Lastly, CNO injection in Cckar^{hM3Dq} animals elevated the core body temperature to the ceiling of the normal physiological range in both intact and OVX females, supporting a role of VMHvll^{Cckar} cells in regulating body temperature in a sex-hormone independent manner (Figures S8G–S8K).

Optogenetic activation of VMHvll^{Cckar} cells facilitates mating and suppresses female aggression

We then tested the sufficiency of VMHvll^{Cckar} cells in promoting female sexual behaviors by expressing ChR2-EYFP in VMHvll^{Cckar} cells (Cckar^{ChR2}) (Figure 5A). The light or sham stimulation started when male attempted to mount (Figure 5B). Upon light delivery, Cckar^{ChR2} but not Cckar^{GFP} females decreased their rejective behaviors, e.g. darting and upright pushing (Figures 5C and 5F). As a result, the male SBS increased (Figures 5l–5J). Overall, the male significantly increased its mounting success and advance the mount to intromission in ~30% of the trials (Figures 5K–5M). When males mounted and intromitted, the SBS of Cckar^{ChR2} females also increased (Figure 5E). However, the females did not assume a clear lordosis posture and wiggled in nearly all trials (Figures 5G–5H). Importantly, the light-induced change in female sexual behavior was not due to reduced movement. In fact, light stimulation promoted locomotion in solitary females (Figure S11A–S11D).

Next, we asked whether optogenetic activation of VMHvll^{Cckar} cells could acutely change aggression in lactating Cckar^{ChR2} females (Figure 5N). The light and sham stimulation started once the female initiated attack towards a juvenile. Upon light delivery, Cckar^{ChR2}, but not Cckar^{GFP} females, immediately aborted attack and never reinitiated it during the remaining light period although the female continued to investigate the juvenile (Figure 5O). Overall, light stimulation significantly shortened latency to stop attack and decreased the total attack time (Figures 5R–5S) while increasing the probability and duration of investigation (Figures 5T–5W). Although activating VMHvll^{Cckar} cells in lactating females clearly suppressed aggression, it failed to promote sexual behavior, further suggesting circuits downstream of VMHvll^{Cckar} cells may be altered during lactation to prevent the occurrence of sexual behaviors (Figures S11E–S11O). In diestrous females, activating VMHvll^{Cckar} cells did not change the duration of juvenile investigation, suggesting that VMHvll^{Cckar} cells do not alter social investigation in general (Figures S11P–S11S). Cckar^{GFP} females showed no change in any behavior during light stimulation in comparison to sham stimulation (Figure 5). Thus, we concluded that acute activation of VMHvll^{Cckar} cells can reduce rejection against males, increase mating success and suppress maternal aggression, but it does not elicit immediate expression of lordosis.

Female VMHvll^{Cckar} cells are activated by males in a reproductive state dependent manner

We next performed fiber photometry recording of female VMHvll^{Cckar} Ca^{2+} activity across reproductive states (Chen et al., 2013) (Figure 6A–6B). We found that the spontaneous Ca^{2+} transients of female VMHvll^{Cckar} cells at the baseline varied significantly with the reproductive state (Figures 6C–6F). Specifically, Ca^{2+} transients occurred more frequently and of a higher magnitude during estrus than diestrus or lactation (Figures 6D–6F).

When a male was introduced into the recording female's home cage, we observed a dramatic increase in Ca^{2+} signal when the female was in estrus (Figures 6G–6I). The increase decayed slowly and the Ca^{2+} signal maintained at an elevated level throughout the recording session (Figures 6G, 6J and 6K). The difference in VMHvl^{Cckar} cell activity was not due to differences in behaviors as the duration of male-female interaction was similar in estrous and lactating females while the cell activity under these two states differed significantly (Figure 6L).

When the male approached the female, VMHvll^{Cckar} cell activity gradually increased especially when the females were in estrus (Figure 6M1). The activity at the approach offset (defined as when the male-female distance reached minimum) and its rise during the last second of approach were significantly higher in virgin females than in lactating females (Figures 6M2-6M3). Similarly, when the female approached the male, VMHvll^{Cckar} cell activity increased and the increase was the highest during estrus (Figures 6N1–6N3). Ca^{2+} activity further increased during male-female close interaction, and the increase was the highest during estrus (Figures 6O and 6P). Behaviorally, diestrous females frequently dart away upon male's contact (Figure S12A–S12B) and VMHvll^{Cckar} cell activity appeared to increase during darting (Figures S12C–S12E). However, we found that Ca^{2+} signal did not increase during "pure" darting events that were not preceded by close male-female interaction, arguing against a role of VMHvll^{Cckar} cells in promoting darting per se (Figures S12F–S12I).

Regardless of the female's reproductive state, VMHvll^{Cckar} cells increased activity when the male attempted to mount, defined as the moment the male physically contacted the back of the female (Figure 6Q). The magnitude of increase was the highest in estrous females (Figure 6Q). The male could try to mount following close interactions or from the rear end of the female without preceding interaction. We found no difference in Ca^{2+} activity between these two scenarios except an earlier rise in Ca^{2+} signal in the former case, likely reflecting the activity increase during close interaction (Figures S12J–S12M). This result suggests that the activity rise during male mounting is likely driven by cutaneous instead of olfactory inputs.

When male mount an estrous female, the female could stay stationary or wiggle. In either case, the activity of female VMHvll^{Cckar} cells gradually decreased from its peak level at mounting onset (Figure 6R, 6S1, 6S2 and 6T1). When we analyzed the Ca^{2+} signal trial-by-trial, we did not observe a within-animal difference in VMHvll^{Cckar} cell activity between wiggling trials and lordosis trials (Figure 6T2).

After male ejaculated, the activity of female VMHvll^{Cckar} cells decreased abruptly (Figures 6S3–6S4) and remained low after male removal (Figures 6U–6X). In contrast, the post-male transient frequency slightly increased from the pre-male level in females that only received intromission (Figures 6W–6X). The decreased VMHvll^{Cckar} cell activity after male ejaculation coincided with decreased female's interest towards males. In the three chamber social preference test, females spent significantly less time with an unfamiliar male post-ejaculation and preferred an unfamiliar diestrous female over male (Figures S13A–S13C). The decreased VMHvll^{Cckar} cell spontaneous activity after ejaculation lasted throughout

pregnancy and lactation and only returned to pre-ejaculation level once the female became estrous again after pups were removed (Figures S13D–S13H).

In a subset of animals, we simultaneously recording GFP and GCaMP6s expressing VMHvll^{Cckar} cells in contralateral sides (Figure S14A). While robust behavior-aligned fluorescence changes were observed from GCaMP6s expressing cells, GFP cells showed minimal changes in fluorescence during all behaviors, suggesting that GCaMP signal change was not due to movement artifacts (Figures S14B–14G). Altogether, these results support that VMHvll^{Cckar} cell activity is highly correlated with female sexual motivation, receptivity and reproductive state.

VMHvll^{Cckar} cells were mostly inhibited by non-male social stimuli

We further investigated VMHvll^{Cckar} cell responses to adult female, juvenile and pups (Figures S15A–S15C). The Ca^{2+} signal increase upon introducing any of these social stimuli was consistently smaller and decayed faster than that to an adult male (Figures S15D–S15H). The sustained elevation in Ca^{2+} signal was also significantly higher with a male intruder than with other intruders especially when the female was in estrus (Figure S15I). When the test female investigated and occasionally mounted the intruder female, VMHvll^{Cckar} cell activity decreased (Figures S15J and S15L–S15O). When female investigated the juveniles, VMHvll^{Cckar} cells increased but to a lesser extent than that during male investigation (Figures S15J–15L). A subset of lactating females attacked juvenile intruders and no activity change was observed during attack (Figures S15P–S15R). Lastly, during pup grooming, VMHvll^{Cckar} cells showed no change in activity or were slightly inhibited (Figures S15J–S15L). Overall, VMHvll^{Cckar} cells are largely unresponsive or inhibited by non-adult male social stimuli or during non-sexual social behaviors.

VMHvll^{Cckar} cell responses to social cues in head-fixed animals

We further compared the cell responses to well-controlled social stimulus presentation in head-fixed recording animals (Figures 7A and 7B) and found significantly higher responses to anesthetized adult male mice than any other social stimuli across all reproductive states (Figures 7C–7K). During estrus, VMHvll^{Cckar} cells showed higher male biased responses than that during diestrus (Figure 7L).

During female investigation and mounting attempts, male emits ultrasonic vocalizations (USVs), which are attractive to conspecific females and facilitate lordosis (Figure 7M) (Pomerantz et al., 1983; Sales, 1972). We thus asked whether VMHvll^{Cckar} cells are responsive to male USVs (Figures 7N–7O) and found that although USVs alone did not evoke an increase in Ca^{2+} signal, it consistently enhanced VMHvll^{Cckar} cell responses to an anaesthetized male mouse, suggesting that female VMHvll^{Cckar} cells could integrate conspecific male cues of multiple sensory modalities (Figures 7P–7R).

Changes in electrophysiological properties of VMHvll^{Cckar} cells over female reproductive cycle

To understand the electrophysiological changes that may underlie *in vivo* response changes, we performed *in vitro* recordings of VMHvll$^{Cckar+Esr1+}$ cells in brain slices obtained from

estrous, diestrous and lactating Cckar^{Cre};Ai9;Esr1^{ZsGreen} female mice (Figure 8A)(Madisen et al., 2010; Saito et al., 2016). Histology analysis revealed a near one-to-one relationship between ZsGreen and Esr1 expression, supporting the utility of the Esr1^{ZsGreen} line to faithfully identify VMHvll^{Esr1} cells (Figures 8B–8C). As virtually all VMHvll^{Cckar} cells express Esr1 (Figure 1D), VMHvll$^{Cckar+Esr1+}$ cells are practically equivalent to VMHvll^{Cckar} cells and will be referred as such.

We first performed cell-attached recordings and found that while VMHvll^{Cckar} cells were spontaneously active during estrus, they rarely spiked during diestrus and lactation (Figures 8D–8F). The nearby VMHvll$^{Cckar−Esr1+}$ cells were generally more active and did not differ in spontaneous firing rate between estrus and diestrus although they did fire less frequently during lactation (Figures 8D–8F). Whole-cell current clamp further revealed a steeper frequency-current (F-I) curve and a significantly higher maximum spiking rate of VMHvll^{Cckar} cells during estrus (Figures 8G–8H, left side). In contrast, nearby VMHvll$^{Cckar−Esr1+}$ cells showed no difference in F-I curve across reproductive states (Figures 8G–8H, right side). Additionally, the resting membrane potential of VMHvll^{Cckar}, but not VMHvll$^{Cckar−Esr1+}$ neurons were more depolarized during estrus (Figure S16A) while neither population changed input resistance over reproductive cycle (Figure S16B).

We further investigated the synaptic inputs onto VMHvll^{Cckar} and VMHvll$^{Cckar−Esr1+}$ using voltage patch-clamp recording. In general, the spontaneous excitatory postsynaptic currents (sEPSCs) were less frequent than spontaneous inhibitory postsynaptic currents (sIPSCs) (Figures 8I, 8J, 8L and 8N). The magnitude of sEPSCs did not change with reproductive state for either population (Figures 8I and 8K) while the frequency of sEPSCs of VMHVll^{Cckar} cells during diestrus was slightly higher than that during estrus and lactation (Figure 8L). The most noticeable change in synaptic input was the heavily reduced sIPSCs of VMHVll^{Cckar} cells during estrus, both in frequency and magnitude (Figures 8J, 8M–8N). The sIPSCs of VMHvll$^{Cckar−Esr1+}$ cells did not differ between estrus and diestrus, but became more frequent and of higher magnitude during lactation, suggesting broader synaptic plasticity during lactation (Figures 8J, 8M–8N). Together, these data revealed unique changes in VMHvll^{Cckar} cell excitability and synaptic transmission over reproductive cycle.

Discussion

VMHvll^{Cckar} cells act as a master control of female sexual behaviors

Functional manipulations at multiple time scales revealed a rich cohort of behaviors that are under the control of VMHvll^{Cckar} cells. First, VMHvll^{Cckar} cells can bi-directionally modulate female's interest towards a male as measured by the female's tendency to approach a male.

Second, VMHvll^{Cckar} cells bi-directionally control female sexual receptivity. This result is similar to that of VMHvl$^{Esr1+Nyp2r−}$, but differs from VMHvl^{Esr1} or VMHvl^{PR} activation which promoted aggression/male-style mounting (Hashikawa et al., 2017a; Inoue et al., 2019; Liu et al., 2022; Yang et al., 2013). Thus, aggression-related VMHvl cells likely dominate the reproduction related-cells if these two populations are simultaneously active.

In comparison to brief optogenetic stimulation, chemogenetic activation of VMHvll^{Cckar} cells, which causes elevated activity for at least 30 minutes, induced a higher increase in receptivity. This result, along with the observation that VMHvll^{Cckar} cells show elevated spontaneous activity during estrus, suggest that the responsiveness of the circuit downstream to the VMHvll^{Cckar} may depend on the accumulated instead of instantaneous VMHvll^{Cckar} cell activity, an idea that had been proposed previously based on electric stimulation results (Pfaff and Sakuma, 1979). However, optogenetic activation of VMHvll^{Cckar} cells does not directly drive lordosis. In fact, the manipulation increased, instead of decreased, locomotion when the female is solitary. Indeed, most activity changes of VMHvll^{Cckar} cells do not occur during lordosis. During male intromission when the female keeps lordotic, VMHvll^{Cckar} cell activity gradually decreases. No trial-to-trial correlation between the occurrence of lordosis and VMHvll^{Cckar} response was found. Thus, although female receptivity, i.e. the probability of lordosis, increases with higher VMHvll^{Cckar} cell activity, VMHvll^{Cckar} cells do not initiate moment-to-moment lordosis.

Third, VMHvll^{Cckar} cell activity bi-directionally modulates core body temperature. This is consistent with previous reports showing that VMH lesion, gene knockdown or estradiol application can influence body temperature (Martinez de Morentin et al., 2014; van Veen et al., 2020). The body temperature increase induced by VMHvll^{Cckar} activation is confined within the normal physiological range, resembling the sustained core body temperature elevation during estrus in the dark phase (Sanchez-Alavez et al., 2011).

Forth, VMHvll^{Cckar} cell activation consistently suppressed female aggression, suggesting that the reproduction circuit, once activated, antagonizes the aggression circuit. However, inhibiting VMHvll^{Cckar} cells did not enhance female aggression. Thus, VMHvll^{Cckar} cells do not exert a tonic inhibition on aggression circuit.

It remains unclear whether VMHvll^{Cckar} cells control each of these behaviors through distinct or overlapping projections. Among all the outputs, VMHvll^{Cckar} projection to AVPV is particularly interesting as it is female- and VMHvll-specific, hence, a unique feature of VMHvll^{Cckar} cells. Optogenetic inhibition of VMHvl^{PR} to AVPV projection reduces female sexual receptivity, supporting this pathway as an essential component in female reproduction circuit (Inoue et al., 2019). Lesioning PAG reduces lordosis while its electric stimulation increases the output of premotor neurons relevant for lordosis and facilitates this behavior in rats (Cottingham et al., 1987; Sakuma and Pfaff, 1979a, b). Polysynaptic retrograde tracing further suggests PAG as a potential intermediator between VMHvl and premotor neurons that control lumbar epaxial muscles for lordosis (Calizo and Flanagan-Cato, 2000). Thus, VMHvl-PAG projection has been proposed as an important pathway for lordosis (Shelley et al., 2006). However, based on our recording and functional results, we speculate that VMHvl does not directly activate lordosis-driving premotor neurons. Instead, it may gate the responses of these cells. During estrus, VMHvll^{Cckar} output increases and opens the gate to permit lordosis reflex in response to male cues. Given the close distance between VMHvll and VMHvlm, VMHvll^{Cckar} cells are well positioned to directly influence VMHvlm aggression cells. However, recent dual VMHvl patch clamp recording suggests sparse inter-VMHvl connection (Shao et al., 2022). Nevertheless, VMHvll^{Cckar} may suppress VMHvlm aggression cell activity indirectly through the surrounding regions,

which contain abundant GABAergic cells and connect with VMHvl cells bi-directionally (Hashikawa et al., 2017b). Lastly, VMHvll^{Cckar} may modulate body temperature via its dense projection to mPOA and DMH, two key regions essential for temperature control (Zhao et al., 2017). Future circuit studies will help further elucidate the functional relevance of each VMHvll^{Cckar} pathway.

The reproductive state dependent changes of VMHvll^{Cckar} cell activity

Why are females only sexually receptive during estrus? This state-dependent behavior change is presumably supported by changes in the reproduction circuit and VMHvll^{Cckar} cells appear to be a key population undergoing changes. Our *in vivo* optical recording demonstrated higher spontaneous activity and male responsivity of VMHvll^{Cckar} cells in estrous females than diestrous and lactating females, likely due to increased cell excitability and decreased inhibitory inputs. The electrophysiological changes of VMHvll^{Cckar} cells are likely supported by molecular changes. Recently, scRNAseq of Esr1+ cells revealed Cckar+ cells in the VMHvl as a homogenous cluster that shows reproductive state dependent transcriptomic changes. Furthermore, the study demonstrated that AVPV terminals originated from VMHvl^{Cckar} cells, but not VMHvl$^{Cckar-Esr1+}$ cells, vary significantly with reproductive state (Knoedler et al., 2022). These results together with our current findings revealed dynamic changes of VMHvl^{Cckar} cells at the molecular, cellular and synaptic levels over estrous cycle, suggesting its unique role in modulating female sexual behaviors in virgins. During lactation, our findings suggest a broader suppression of reproduction circuit which combines with an increased activity in the aggression circuit (Liu et al., 2022) leads to a total switch from sexual behaviors to aggression (Figure S17A).

One relevant question is whether CCK-Cckar signaling modulates VMHvll^{Cckar} cell activity during estrous cycle. We speculate this may be the case. First, exogenous CCK can influence female sexual behaviors. Intraperitoneal injection of CCK or local infusion of CCK into mPOA facilitates female sexual behaviors in non-receptive rats (Bloch et al., 1987; Dornan et al., 1989) although somewhat surprisingly, CCK injection into VMH suppresses receptivity (Babcock et al., 1988). Second, Cckar-null female mice are less receptive than control mice (Xu et al., 2012). Third, the expression of CCK and Cckar are profoundly modulated by estrogen and vary during the estrous cycle, both with higher values during estrus than diestrus (Frankfurt et al., 1986; Kim et al., 2019; Knoedler et al., 2022; Oro et al., 1988). As Cckar is primarily coupled to Gq and *in vitro* CCK application increases VMHvl cell activity (Kow and Pfaff, 1986; Liu et al., 2021), an increase in CCK release and Cckar expression during estrus is expected to increase VMHvll^{Cckar} cell activity. Taken together, we speculate that CCK release as well as Cckar expression in the VMHvll will increase during estrus due to changes in sex hormones, which could lead to an increase in spontaneous activity of VMHvll cells. Beyond a role in enhancing baseline activity, CCK may also be released in the VMHvll during male interactions to acutely increase VMHvll^{Cckar} cell activity. Although the source of CCK to VMHvll is unknown, both MeA and BNST project heavily to the VMHvll and are enriched of CCK (Canteras et al., 1995; Dong and Swanson, 2004; Micevych et al., 1988).

The placement of VMHvll^{Cckar} cells in the reproduction circuit

Based on the response profile of VMHvll^{Cckar} cells and the behavioral consequences of VMHvll^{Cckar} manipulations, we propose a role of VMHvll^{Cckar} cells in reproduction similar to that of AgRP cells in the arcuate nucleus (ARC^{AgRP}) in feeding. Numerous studies established ARC^{AgRP} as hunger cells, cells that signal the drive for food (Andermann and Lowell, 2017; Sternson et al., 2013; Zimmerman and Knight, 2020). In the same vein, we consider VMHvll^{Cckar} cells as the neural substrate for sexual motivation (Figure S17B). ARC^{AgRP} and VMHvll^{Cckar} show similarity in response patterns and behavioral functions in many ways. On one hand, ARC^{AgRP} and VMHvll^{Cckar} cells respectively sense various feeding- and reproduction-related internal and external cues. On the other hand, both populations promote flexible behaviors depending on the context, e.g. availability of the target, with a goal of increasing reproduction (or feeding) success (Andermann and Lowell, 2017; Sternson et al., 2013; Zimmerman and Knight, 2020). Additionally, both VMHvll^{Cckar} and ARC^{AgRP} cells are capable of suppressing competing motivated behaviors, such as aggression (or foraging risk), and coordinating neuroendocrine and autonomic responses (Burnett et al., 2016). Future experiment should address whether VMHvll^{Cckar} cells, like ARC^{AgRP} cells, can increase efforts in an operant task for mating opportunities, facilitate learning or modulate cortical responses to male associated cues (Berrios et al., 2021; Krashes et al., 2011; Livneh et al., 2017).

What is the utility of neural substrates dedicated for motivation? One explanation, first proposed by Neal Miller and later refined by Berridge, is that motivation is an intervening variable to simplify the link between stimuli (independent variables) and behavior responses (dependent variable) (Berridge, 2004; Miller, 1971). When there is one specific behavioral response to one specific stimulus, the circuit wiring is straightforward and intervening variable is not needed. However, when a large set of possible behaviors can be expressed depending on a combination of multiple stimuli, the complexity of the circuit diagram rapidly explodes. An intervening variable, which integrates many sensory inputs and influences many behavioral outputs, could effectively solve this issue and simplify the circuit. ARC^{AgRP} cells have been suggested as the physical embodiment of an intervening variable for feeding (Andermann and Lowell, 2017) and here, we propose VMHvll^{Cckar} cells as the intervening variable for female reproduction (Figure S17B). These motivation-encoding brain regions orchestrate a wide range of goal-bounded behaviors and represent key sites of intervention under pathological conditions.

STAR★METHODS

RESOURCE AVAILABILITY

Lead contact—Further information and requests for resources and reagents should be directed to and will be fulfilled by the lead contact, Dr. Dayu Lin (dayu.lin@nyulangone.org).

Materials availability—New transgenic mouse lines generated for this study will be deposited at Jackson laboratories upon publication. Probe sets used for double in situ hybridization are listed in METHOD DETAILS, and probe sets used for triple in situ

hybridization are available from RNAscope (ACD; Advanced Cell Diagnostics). This study did not generate new unique reagents not listed here.

Data and code availability

- All data reported in this paper will be shared by the lead contact upon request.
- This paper does not report original code. All Matlab code used in this manuscript are available from the lead contact upon request.
- Any additional information required to reanalyze the data reported in this paper is available from the lead contact upon request.

EXPERIMENTAL MODEL AND SUBJECT DETAILS

Mice—All procedures were approved by the NYULMC Institute Animal Care and Use Committee (IACUC) and the Institute Biosafety Committee (IBC) in compliance with NIH guidelines for the care and use of laboratory animals. All mice in this study, including wild-type and transgenic mice, were bred at NYULMC animal facility. All mice were housed under a reversed 12 h light-dark cycle (10 p.m. to 10 a.m. light), with food and water available ad libitum. Single-housed virgin $Cckar^{Cre}$, $Cckar^{Cre}$;Ai6 and $Cckar^{Cre}$;Ai9;$Esr1^{ZsGreen}$ female mice (2–6 months) were used as experimental mice. For functional manipulation and *in vivo* recording experiments, we tested the same set of females across reproductive states. After completing the tests in virgin females, they were paired with males. Once they became visibly pregnant, the male mouse was removed. The first day pups were found was counted as postpartum day 1 (P1), behavioral tests in lactating females were conducted between P3 and P6, and pups were euthanized after P7. Single-housed sexually experienced male (3–12 months), group-housed female mice (2–6 months), group-housed male juvenile (postnatal day 15–25), and pup (postnatal day 1–7, housed with mom) were used as social stimuli.

$Cckar^{Cre}$ mice were generated in this paper, firstly in Swiss Webster background and then backcrossed into C57BL/6 background for at least seven generations. All the other transgenic animals were with C57BL/6 background. Ai6 mice were purchased from the Jackson Laboratory (stock no. 007906). Ai9 animals were generously provided by Dr. Bernardo Rudy, but also available from Jackson lab (stock no. 007909). $Esr1^{ZsGreen}$ mice were generated and kindly provided by Dr. Yong Xu's lab (Saito et al., 2016). Heterozygote $Cckar^{Cre}$, double heterozygote $Cckar^{Cre}$;Ai6, or triple heterozygote $Cckar^{Cre}$;Ai9;$Esr1^{ZsGreen}$ female mice were used for cell-specific targeting, visualizing Cckar cells and *in vitro* slice recording, respectively. Animals were genotyped by PCR analysis using genomic DNA from tail tissue.

METHOD DETAILS

Viruses and retrograde tracer—AAV1-hSyn-DIO-hM4Di-mCherry (2×10^{13} genomic copies per ml), AAV2-hSyn-DIO-hM3Dq-mCherry (2×10^{13} genomic copies per ml), AAV2-hSyn-DIO-mCherry (1.8×10^{13} genomic copies per ml), AAV1-hSyn1-SIO-stGtACR2-FusionRed (2.1×10^{13} genomic copies per ml), and AAV1-hSyn-Flex-GCaMP6s-WPRE-SV40 (1.6×10^{13} genomic copies per ml) were purchased from Addgene. AAV2-EF1a-DIO-

ChR2-EYFP (4×10^{12} genomic copies per ml) and AAV2-CAG-Flex-GFP (4×10^{12} genomic copies per ml) were purchased from the University of North Carolina vector core. Red retrobeads was purchased from Lumafluor, Inc (Red Retrobeads™).

Drugs—For chemogenetic activation in freely behaving mice, Clozapine N-oxide (CNO, Sigma-Aldrich C0832) was dissolved in 0.2 mL vehicle solution (PBS with 0.3% DMSO) and administered intraperitoneally (1 mg/kg). Ketamine (100 mg/kg) with xylazine (10 mg/kg) were dissolved in PBS and injected into stimulus animal intraperitoneally in headfixed fiber photometry recording experiment.

Generation of Cckar^{Cre} mice—The Cckar^{Cre} mouse was generated at NYULMC Rodent Genetic Engineering Laboratory by homologous recombination at the endogenous Cckar locus utilizing Easi-CRISPR technology (Miura et al., 2018). Briefly, single-stranded DNA (ssDNA) donor containing homology arms of Cckar locus flanking T2A-Cre sequence, which was inserted just before the endogenous STOP codon, was commercially synthesized (Integrated DNA Technologies, IDT) (Figure S1). To generate a site-specific double stranded break with Cas9, a targeting sequence, crRNA sequence, was designed using an online guide RNA designing tool (https://zlab.bio/guide-design-resources) and commercially synthesized (Integrated DNA Technologies, IDT) (Figure S1). On the day of microinjection, ssDNA donor (10 ng/ul), CRISPR components (crRNA, tracrRNA (20 ng/ul), and Cas9 protein (20 ng/ul) were mixed and microinjected into fertilized zygotes from Swiss Webster females. Injected zygotes were implanted into oviducts of pseudopregnant CD1 female mice (Charles River Lab). Any potential off-target effects were bred out by backcrossing to C57BL/6 mice for at least 7 generations before using for experiments. The PCR mutant forward primer is: AACTGGTCGAGCGATGGATTT; wildtype forward primer is: GATCCGCATGCTCATTGTCATT (498 bp); common reverse primer is: AAAGCAGACATCGGAAGAGTCC (476 bp).

Double in situ hybridization—10–12-weeks-old C57BL/6 female mice that were anesthetized with a mixture of ketamine (100 mg/kg) and xylazine (10 mg/kg) and transcardially perfused with 10 ml of DEPC treated PBS (DEPC-PBS), followed by 10 ml of 4% PFA in DEPC-PBS (Electron Microscopy Sciences). After perfusion, brains were harvested, soaked in 30% of sucrose in DEPC-PBS for 24 hours at 4°C and then embedded with O.C.T compound (Fisher Healthcare). 20 μm thick coronal brain sections were cut using a cryostat (Leica) and stored at −80°C until use.

To synthesize the cDNA for the *Cre* and *Cckar* probes, their original templates were from DNA plasmid including Cre sequence and mouse brain cDNA (cDNA-mmu-01, BiOSETTIA) respectively. cDNA were amplified by PCR methods using the following oligo-DNA primers and the products were purified with micro spin columns (MACHEREY-NAGEL, 74060910). Each reverse primer also possesses T3 sequence for transcription.

The *Cre* probes are approximately 800 bp in length and consist of 3 probes to cover nearly the full length mRNA. The primer sequences for making the *Cre* probes are:

Cre1-forward: TGCAACGAGTGATGAGGTTC

Cre1-reverse: AATTAACCCTCACTAAAGGGTTTCACTATCCAGGTTACGG

Cre2-forward: GGTGCAAGTTGAATAACCGG

Cre2-reverse: AATTAACCCTCACTAAAGGGTGACCAGAGTCATCCTTAGC

Cre3-forward: GCGGTCTGGCAGTAAAAACT

Cre3-reverse: AATTAACCCTCACTAAAGGGCGCTCGACCAGTTTAGTTAC

The *Cckar* probes are approximately 500 bp in length and consist of two probes to cover the 4th exon of *Cckar* mRNA:

Cckar1-forward: TGCTCCTGAAGAATTCTGGTCC

Cckar1-reverse: ATTAATACGACTCACTATAGGGAGGCATTTCTGGAAAGGAGGA

Cckar2-forward: CTGCCAAGTCCACGTTCAAAAT

Cckar2-reverse: ATTAATACGACTCACTATAGGATCATCCTTCTGCAGCTTGACA

Cckar probes were labeled with DIG (Roche Applied Science, #11277073910) and *Cre* probes were labeled with Fluorescein (Roche Applied Science, #11685619910). Brain sections underwent hybridization at 56°C overnight. Then, after a series of post-hybridization washing and blocking, fluorescein was visualized with anti-FITC antibody (PerkinElmer, #NEF710001EA, 1:200 in blocking buffer) followed by TSA biotin amplification (PerkinElmer, #NEF749A001KT, 1:100 in 1×plus amplification diluent) and streptavidin Alexa488 (Invitrogen, #S11223, 1:250 in blocking buffer). DIG was visualized with anti-DIG antibody (Roche Applied Science, #11207733910, 1:250 in blocking buffer) and followed by TSA Cy3 amplification (PerkinElmer, #NEL744001KT, 1:70 in 1×plus amplification diluent).

Triple in situ hybridization using RNAscope—Extracted brains were frozen on dry ice and 18-μm coronal brain sections were collected using a cryostat (Leica Biosystems). Triple labeling of *Cckar*, *Npy2r* and *Esr1* was performed following the manufacturer protocol (ACD; Advanced Cell Diagnostics)(Wang et al., 2012). In brief, sections were treated with a series of ethanol and protease digestion followed by hybridization with a mixture containing target probes to mouse Cckar (313751-C3), Npy2r (315951-C2), and Esr1–1 (432861). Sections were then cover slipped using 50% glycerol containing DAPI (Invitrogen, Cat. #00-4959-52) and imaged with a confocal microscope (Zeiss LSM 800). A cell was considered as probe+ if it contained >2 fluorescence spots and is DAPI+.

Immunohistochemistry and imaging analysis—Mice were perfused with 1×PBS followed by 4% PFA. Brains were harvested, post-fixed in 4% PFA overnight at 4°C, rinsed with 1×PBS and dehydrated in 30% sucrose for 24 hours. 50 μm sections were cut on a cryostat (Leica CM1950). For quantification of Cckar cell distribution in male and female along the anterior-posterior axis, all VMHvl sections were collected. For Fos/Esr1 staining, every other sections was collected. Free-floating brain sections were then rinsed with PBS

(3×10 min), PBST (0.3% Triton X-100 in PBS, 1×30 minutes), blocked with 5% normal donkey serum (Jackson ImmunoResearch, Code: 017-000-121, RRID:AB_2337258) at room temperature and incubated with primary antibody (guinea pig anti-Fos, 1:1000 dilution, Synaptic Systems, Cat. # 226005, RRID:AB_2800522; or goat anti-Fos, 1:1000 dilution, Santa Cruz Biotechnology, Cat# sc-52-G, RRID:AB_2629503; rabbit anti-Esr1, 1:1000 dilution, Millipore, Cat. # 06-935, RRID:AB_310305) in PBST containing 5% normal donkey serum overnight (12–16 hours) at 4°C. Brain sections were then washed with PBST (3×10 min), incubated with the corresponding secondary antibody (Secondary antibody for Fos staining, Cy3-goat anti-Guinea pig, 1:1000 dilution, Jackson ImmunoResearch, Cat. # 706-165-148, RRID:AB_2340460; Secondary antibody for Fos staining, 488-donkey anti-Goat, 1:1000 dilution, Jackson ImmunoResearch, Cat. # 705-545-147, RRID: AB_2336933; Secondary antibody for Esr1 staining, Cy5-goat anti-Rabbit, 1:1000 dilution, Jackson ImmunoResearch, Cat. # 711-175-152, RRID:AB_2340607) for 2 hours at room temperature, washed with PBST (3×10 min), PBS (2×10 min), and then mounted (Fisher Scientific, 12–550-15) and cover slipped using 50% glycerol containing DAPI (Invitrogen, Cat. #00-4959-52). Images were acquired using slide scanner (Olympus, VS120) or confocal microscope (Zeiss LSM 800). Brain regions were identified based on Allen Mouse Brain Atlas, and cells were manually counte using Adobe Photoshop (Adobe, RRID:SCR_014199). To quantify the distance of Cckar cell to lateral edge of the brain in Figure S2D, we first manually drew a line along the ventral most brain surface vertical to the line along the mediodorsal-ventrolateral axis of the VMH, then used custom-written Matlab code to get the x and y coordinates of each ZsGreen positive cells and thereafter the distance of the cell to the line.

For population A and population B, if they do not overlap preferentially, the percentage of A+ cells in B should be the same as A+ in the total population. Thus, the chance level of (A+B+)/B+, as indicated by dashed lines in Figures 1D, F and H, is equal to A+/DAPI+.

Axon projection mapping—To analyze the projection pattern of VMHvll^{Cckar} neurons, every one in three brain sections (50 μm in thickness) of the whole brain were collected. Sections were fully washed in PBS, mounted and coverslipped using 50% glycerol containing DAPI (Invitrogen, Cat. #00-4959-52). Images were acquired using confocal microscopy with a 10x objective (Zeiss, LSM 800). Brain regions were identified using Allen Mouse Brain Atlas as a reference, except lateroanterior hypothalamic nucleus (LA), which was identified from The Mouse Brain, 3rd edition, and projection patterns were analyzed using ImageJ (ImageJ, RRID: SCR_003070). In detail, for each animal, all images were first thresholded to eliminate the background. We then selected 2–5 regions of interest (ROIs) for each brain region and calculated the average pixel value of each ROI, subtracting the background (averaged pixel value from an ROI that contains no obvious fibers) from it, to obtain the fluorescence density of the ROI. For each animal, the average fluorescence density of a brain region was then calculated as the averaged fluorescence density of all the ROIs within that brain region. The fluorescence density of each region was then normalized by the value of AVPV and then averaged across animals.

Reproductive cycle monitoring—To assess the reproductive state of naturally cycling female mice, vaginal cytology samples were collected 30 minutes before the behavior test or 1 hour before collecting brain slice for *in vitro* recording experiments. We gently flushed 10 μl saline into the vagina using a pipette for three to four times to collect vaginal lavage. Attention was paid to not touch the vaginal wall to avoid cervical stimulation. The flush was then transferred to a glass slide and coverslipped. They were observed under a Zeiss AxioScope A1 bright field microscope with a 10x objective and staged based on the proportion of each cell type in the smear (Ajayi and Akhigbe, 2020).

Stereotactic Surgery—Mice (8–15 weeks old) were anesthetized with 1% isoflurane and placed on a stereotaxic device (Kopf Instruments Model 1900). Viruses were delivered into brains through a glass capillary using nanoinjector (World Precision Instruments, Nanoliter 2000). Female mice were group housed for two to three weeks after virus injection, and then switched to single house one week prior to testing.

For retrograde tracing, we injected diluted retrobeads (1:3 in saline) unilaterally at two depth to cover the entire dorsal-ventral span of AVPV (AP: −0.10 mm, ML: −0.10 mm, DV: −4.80 mm and −5.00 mm, 40 nl per depth) using $Cckar^{Cre}$;Ai6 female mice. Female mice were single housed after injection and tested for behavior one week later. One hour after completing the test, animals were perfused and brains were collected. For anterograde tracing of $VMHvll^{Cckar}$ cells, 30 nl AAV2-CAG-Flex-GFP was unilaterally injected into VMHvll (AP: −1.70 mm, ML: −0.8 mm, DV: −5.66 mm). For chemogenetic activation of $VMHvll^{Cckar}$ neurons, 50 nl AAV2-hSyn-DIO-hM3Dq-mCherry were bilaterally injected into VMHvll of $Cckar^{Cre}$ female mice. Control mice were injected with 50 nl AAV2-hSyn-DIO-mCherry. For chemogenetic inhibition of $VMHvll^{Cckar}$ neurons, 40 nl AAV1-hSyn-DIO-hM4Di-mCherry were bilaterally injected into VMHvll of $Cckar^{Cre}$ female mice. Control mice were injected with 40 nl AAV2-hSyn-DIO-mCherry. For optogenetic activation or inhibition of $VMHvll^{Cckar}$ neurons, 70 nl AAV2-EF1a-DIO-ChR2-EYFP or AAV1-hSyn1-SIO-stGtACR2-FusionRed was bilaterally injected into VMHvll. Control animals were injected with 30 nl of AAV2-CAG-Flex-GFP. After virus injection, 200-μm optical fiber (Thorlabs, FT200EMT) was bilaterally inserted 300 μm above the virus injection site and secured on the skull using adhesive dental cement (C&B Metabond, S380). A headfix ring was then cemented on the skull to help secure animal on the running wheel and alleviate stress during fiber connection and disconnection. For fiber photometry recording of $VMHvll^{Cckar}$ neurons, 60 nl AAV1-hSyn-Flex-GCaMP6s was unilateral injected into VMHvll. To understand fluorescence changes due to motion artifact, in some animals, we injected 30 nl AAV2-CAG-Flex-GFP and 60 nl AAV1-hSyn-Flex-GCaMP6s into the left and right hemisphere, respectively, and recorded the signals simultaneously. To minimize tissue damage, we used 100-μm multimode optical fiber (Doric Lenses, 100 μm-core, 0.37 NA). The fiber was inserted and glued to a guiding groove of a connector (USCONEC, C12405, Ferrule_48F), polished and then inserted into the brain 50 μm above the virus injection site (Sych et al., 2019). The connector was secured on the skull using adhesive dental cement (C&B Metabond, S380). A headfix ring was then secured on the skull. In earlier experiments, we tried AAV1-hSyn-Flex-GCaMP6f and 400-μm optic fiber and found that

the signals were unstable over time and our histology analysis revealed low virus expression possibly due to cell death.

Behavioral analyses—All animal behaviors were video recorded from both the side and the top of the cage using two synchronized cameras (Basler, acA640–120gc) and commercial video acquisition software (StreamPix 8, Norpix, RRID:SCR_015773) in a semi-dark room with infrared illumination at a frame rate of 25 frames/s. Manual behavioral annotation was performed on a frame-by-frame basis using custom software written in Matlab (https://github.com/pdollar/toolbox).

During female-male interaction, we manually annotated the following behaviors of the male intruder: approach, investigation, mount attempt, mount, intromission and ejaculation. For the same video, we also annotated the following female behaviors: approach, investigation, stay, upright, resist, dart, lordosis and wiggle. 'Approach' (either male toward female or female toward male) was annotated when one animal faced the target animal and walked to it without pausing. 'Investigation' was defined as active nose contact to any part of the body of the target animal. 'Mount attempt' was characterized by the male extended its forelimbs to grasp the female's flanks. 'Mount' referred to the period when the male was on top of the female and held the female's lower back using his forelimbs. 'Intromission' was defined as deep rhythmic thrust following mount. 'Ejaculation' was detected when the male stopped deep thrusting for a few seconds while continuously clutching onto the female and then slumping to the side of the female. 'Stay' was annotated when the female quietly stayed in place while male was investigating her or attempting to mount. 'Upright' was defined as female standing up to conceal the anogenital area when male was investigating. 'Resist' was defined as female pushing or kicking the male. 'Dart' was defined as female quickly running, often upon male investigation or mount attempts. 'Lordosis' was defined as female being on the ground and motionless or showing an arched back posture when the male was mounting or intromitting. The 'lordosis quotient' was calculated as the ratio between lordosis events and male mounts. 'Wiggle' was defined as female continuously moving her head or body when the male was mounting or intromitting. Lordosis and wiggle were annotated only during male mounting and intromission. The sum of lordosis and wiggle durations equals to the total male mounting and intromission duration. Under natural conditions, chemogenetic, and fiber photometry experiments, for each mounting/intromission event, if a female stayed stationary for majority of time, the trial was annotated as "lordosis". If the female moved forward or tried to twist its body for majority of time, it was annotated as "wiggle". The sum of lordosis trial% and wiggle trial% is 100%. In ChR2 and stGtACR2 experiments, as the behavior changes acutely with light, we annotate wiggle and lordosis for each frame instead of each trial. We consider the female receptivity level as: lordosis>wiggle>dart away. When females dart away, males cannot achieve successful mount. When females are highly receptive, they show lordosis to facilitate male mounting. Wiggle is an in-between situation. The female allows the male to mount but is not fully cooperative. Thus, when a female changes its behavior from dart away to wiggle, we consider wiggle as an indication of increase in receptivity. This increase makes it possible for the male to achieve mounting. When a female changes its behavior from lordosis to

wiggle, we consider it as an indication of decreased receptivity. This decrease makes it harder for males to achieve intromission after successful mounting.

During female-female interaction, we annotated ‘investigation’ and ‘mount’ expressed by the resident (test) females. ‘Investigation’ was defined as active nose contact to any part of the body of the intruder. ‘Mount’ was defined as when the test female clasped the flank of the intruder female and moved its pelvis back and forth. During female-juvenile interaction, we annotated ‘investigation’ and ‘attack’ expressed by the test female. ‘Attack’ was defined as a suite of actions, including pushes, lunges, bites, tumbling and fast locomotion episodes between such movements. During female-pup interaction, we annotated pup retrieval and pup grooming expressed by the test female. ‘Pup retrieval’ was defined when the female lifted the pup using her jaw to the moment when the pup was dropped in or around the nest. ‘Pup grooming’ was defined as close female and pup interaction that was accompanied by rhythmic up and down head movement of the female and displacement of the pup.

We categorize female receptivity during estrus into three levels, from high to low, as estrus-fully receptive, estrus-semi receptive and estrus-non receptive. ‘Fully receptive’ females are those displayed lordosis posture in over 50% of male mounting trials (LQ>=0.5). ‘Semi-receptive’ females are those showing lordosis in some but less than 50% of male mounting trials (0<LQ<0.5). ‘Non-receptive’ females are animals that did not show lordosis when males forced mount (LQ = 0).

Three Chamber social preference test—The test arena (L×W×H: 50 cm ×18 cm×38 cm) were evenly divided into three compartments with a 6-cm wide opening between the neighboring compartments. All test and stimulus animals were habituated to the chamber for at least two days, 30 minutes each day at non-overlapping time. To test female’s social preference between male and female, on the day of testing, an adult C57BL/6 sexually experienced adult male mouse and a C57BL/6 adult diestrous female mouse was each placed under a wire cup positioned in one of the side compartment, the stimulus animal’s deposits were placed around the cup (< 0.5 cm away) as additional olfactory cues. Then, the testing estrous $Cckar^{hM4Di}/Cckar^{mCherry}$ or diestrous $Cckar^{hM3Dq}/Cckar^{mCherry}$ female was introduced into the middle compartment, and allowed to explore freely for 20 min. A preference score was calculated by dividing the differential time the test female spent on investigating the male and female chamber by the total time spent on investigating both chambers. A positive value indicates preference directed toward the stimulus male, whereas a negative value indicates preference directed toward the stimulus female. For chemogenetic experiment, each animal was tested for the preference test twice on the same day with one hour in between. The first test was performed 30 minutes after intraperitoneal saline injection and the second test was 30 minutes after 1 mg/kg CNO injection. We also used the same test area to compare females’ social interest toward a male before and after being ejaculated. In the test, an adult C57BL/6 female was placed into the middle compartment and allowed to freely explore an unfamiliar sexually experienced male and an unfamiliar diestrus female for 20 minutes. The stimulus animals were placed under wired cups, each in one of the end chambers. Then, the C57BL/6 female was introduced into the home cage of a different male until the male achieved ejaculation. We then put the female back into the same test chamber, and recorded for another 20 min.

The same test area was used for evaluating female's attractiveness to males. All animals were habituated to the area as mentioned above. Two estrous Cckar^{hM4Di} or two diestrous Cckar^{hM3Dq} female mice were used as stimulus animals. Each was placed under a cup that was located in one of the side chamber. Either both stimulus females received saline injection or one stimulus female received CNO injection and the other received saline injection, all at 30 minutes before the testing. The deposits of each stimulus animal were placed around the wire cup. During the test, a sexually experienced unfamiliar male was introduced into the middle chamber and allowed to freely explore for 20 minutes. We used the same male after saline-saline and after CNO-saline injection to eliminate individual variability. A preference score was calculated by dividing the differential time the male spent on visiting the two side chambers by the total time the male spent in both chambers. A positive value indicates preference of the CNO-injected female, whereas a negative value indicates preference of the saline-injected female.

Core body temperature recording—Core body temperature was monitored using a Nano-T temperature logger and analyzed with Mercury Software (Star-Oddi). The logger was implanted in the abdominal cavity and attached to the inside of the body wall. All test mice were singly housed. Parameters of the Logger were set before implantation. To save battery, data acquisition only occurred from 11 am to 5 pm (dark phase of the animal) every other day with a sampling rate of once every 2 minutes. Saline and CNO were injected in a randomized order at 1 pm on separate days.

Chemogenetic activation and inactivation—Due to the high variability of sexual behaviors in estrous females (Figure S4), changes in female sexual behaviors were determined as the difference before and after drug injection on the same day. In detail, on the testing day, we examined female's vaginal smear 30 minutes prior to the pretest. During the pretest, a sexually experienced male was introduced into the homecage of the female for approximately 10 minutes. If the male did not attempt to mount for at least 10 times during the first 10 minutes, the test was extended until the male made 10 mounting attempts or up to 30 minutes, whichever happened first. No males achieved ejaculation during pretest. After the pretest, the male was removed and the female was left alone for an additional 5 minutes and then the female was received either saline or 1 mg/kg CNO i. p. injection. 30 minutes after the injection, we introduced a different sexually experienced male into the female's home cage for 10 minutes or until the male attempted to mount for 10 times. We did not use the same male considering that the same male would be sexually eager after the pretest and may confound the results. 5 minutes after removing the male, we introduced a male juvenile (P15-25) for 10 minutes, an adult female for 10 minutes, and a pup (P1-P7) for 5 minutes, with 5 minutes in between. The order of CNO and saline administration was counter balanced across animals.

Optogenetic activation and inactivation—For optogenetic activation, only diestrous females were used. The estrous state of the Cckar^{ChR2} or Cckar^{GFP} females were determined based on vaginal cytology. For optogenetic inactivation, only fully receptive estrous females were used. The estrous female was tested briefly (<2 min) with a sexually experienced male to ensure her behavioral receptivity.

Before each testing session, a 200-μm patch cord was coupled to the implanted fiber assembly with a ceramic split sleeve (Thorlabs, ADAL1-5). The patch cord was connected to a 473-nm blue laser (Shanghai Dream Lasers Technology, SDL-473-100MFL). A custom written TDT circuit was used to generate TTL pulses to control the laser output and synchronize it with the behavior video. The circuit also generated a constant TTL signal to drive an LED indicator when the light pulse or sham light was delivered.

To test the effect of optogenetic activation of VMHVll^{Cckar} cells on female sexual behavior, we manually triggered the light when the male attempted to mount the diestrous female. Each light stimulation lasted for 20 seconds (3 mW, 20 ms, 20 Hz) and was interleaved with sham (0 mW) trial. We collected ~10 stimulation and ~10 sham trials during each recording session from each animal. To test the effect of optogenetic activation on maternal aggression, we delivered the light and sham light to the lactation females (P3 to P6) as soon as she initiated attack towards a juvenile male mouse (P15-P25). To collect sufficient attack trials, we replaced the juvenile if the test female ceased attack after several minutes of interaction. All the pups were removed right before the test. To test the effect of optogenetic activation on female investigation towards a juvenile, we delivered the light and sham light to the diestrous test female when she investigated a juvenile male mouse (P15-P25) for ~2 seconds. To test the effect of the optogenetic inactivation on female sexual behavior, we manually triggered the light when the male successfully mount the estrous female. Each light stimulation lasted for 10 seconds (5 mW, continuous light) and was interleaved with sham (0 mW) light delivery.

To quantify the instantaneous change in sexual behaviors induced by the light, we calculated frame-by-frame sexual behavior score (SBS) as following. For female sexual behaviors, a frame that was annotated as lordosis was assigned a value of 2, wiggle as 1 and other behaviors as 0. For male sexual behaviors, we assigned intromission frame as 3, mount as 2, attempt mount as 1 and others as 0. PSTHs of SBS aligned to the onset of light or sham stimulation was then constructed for each animal and then averaged across animals.

Animal body tracking—The behavior was recorded using a top-view camera and the location of the animal was tracked and analyzed using custom-written Matlab code (https://github.com/pdollar/toolbox)(Lin et al., 2011).

Fiber photometry—Virgin Cckar^{Cre} females aged 8–15 weeks were used for surgery and the recording started four weeks after surgery. Estrous and diestrous states were determined by vaginal cytology. For females that were first recorded during estrus, we ensured that the male did not achieve ejaculation during the recording. For those females, once the recording under diestrus was completed, the females were recorded again during estrus and the male was allowed to achieve ejaculation. For all analysis in Figures 6E–6Q, the recordings under estrus and diestrus were spaced for no more than 4 days. After a female was ejaculated, it was kept in the animal facility and checked daily. The first day when pups were found was counted as postpartum day 1 (P1). Behavioral tests in the lactating state were conducted on P3 to P6. Among the 9 recording animals with correct VMHvll targeting, two failed to become pregnant and thus their data during lactation were not available. Of note, during our fiber photometry recording, Cckar^{Cre} C57 lactating females rarely attacked

adult intruders and thus the cell responses to males in lactating females were unrelated to maternal aggression.

The optical recording setup was a modified version described in previous studies (Falkner et al., 2016; Kim et al., 2016; Sych et al., 2019). Briefly, blue LED light (Thorlabs, M470F1, LEDD1B) was bandpass filtered (Semrock, FF02-472/30-25), reflected on a dichroic filter (Semrock, FF495-Di03-25×36), and coupled into a custom designed 100-μm fiber bundle (Doric Lenses) through an Olympus PLN 10x objective (Edmunds, Stock #86-813). Emission light was bandpass filtered (Semrock, FF01-535/50) and projected onto the CCD sensor of a camera (Basler, acA640-120gc) via an achromatic doublet (Thorlabs, AC254-060-A-ML). The LED was driven by DC current, and the light intensity at the tip of the fiber was set to be ~30 μW. The sampling rate of the camera was 25 frames/s.

During each recording day, female was first left alone in home cage for 5 minutes, then a sexually experienced mounter was introduced for 20 min or until male achieved ejaculation. An adult female, a juvenile male (P15-P25), and a pup (P1-P7) was then introduced sequentially, each for 10 minutes except pup, which was for 5 minutes, with a 5-minute break in between. We recorded the top-view and side-view of behavior and the Ca^{2+} signal from the optic fiber end using three synchronized cameras (acA640-120gc GigE camera) at 25 Hz frame rate using Streampix 8 (Norpix inc). Timestamps of each video frame were recorded and checked offline to ensure synchronization. In cases where frames were skipped or jittered, time stamps were used to realign the videos to ensure that corresponding frames from all camera were collected within 40 ms.

After video acquisition, we selected regions of interest (ROI) encompassing the optic fiber end and calculated the mean fluorescence value of all pixels within the ROI as the raw Ca^{2+} signal for each frame. The Matlab function “msbackadj” with a moving window of 25% of the total recording duration was then applied to the raw signal to obtain the instantaneous baseline signal. The instantaneous ΔF/F was then calculated as (Fraw−Fbaseline)/Fbaseline. Then, for each animal, we obtained the normalized ΔF/F by dividing the ΔF/F in each frame by the maximum ΔF/F across all the recording days. The normalized ΔF/F ranged from 0–1 for each animal and was used for all subsequent plotting and statistical analysis. The peak ΔF/F was calculated as the maximum normalized ΔF/F during a behavior. The change in ΔF/F during a behavior was calculated as the peak (if the signal was upward) or the trough if the signal was downward, of the normalized ΔF/F 0 to 2 s after the behavior onset, minus the mean normalized ΔF/F −3 to −1s preceding the behavior. For Figure 6S4, each value was calculated as the mean normalized ΔF/F of all episodes of a behavior for each animal. The entry peak ΔF/F for each stimulus was calculated as the maximum normalized ΔF/F between 0 and 60 s after the stimulus introduction. The sustained ΔF/F was calculated as the average normalized ΔF/F from 60 s to 600 s after the male introduction for Figure 6G or from 60 s to 300 s after introduction of various stimulus for Figures S15D–S15F.

To quantify the frequency and magnitude of spontaneous Ca^{2+} transients when female was alone in her home cage, we identified all the peaks and preceding troughs in the recorded traces (normalized ΔF/F) using Matlab function “findpeaks”. The difference between each

pair of trough and peak was calculated as the magnitude of a transient. Transients with magnitude above 1.5 × standard deviation of the whole trace were included for analysis.

To better control the stimulus, we also performed fiber photometry recording on headfixed animals. In short, we head fixed the recording female using a 3D-printed head ring and placed it on a running wheel (Osborne and Dudman, 2014). The stimulus animal was anesthetized with ketamine (100 mg/kg) and xylazine (10 mg/kg) and placed onto a movable plastic board. When the board was moved to its ending position, the nose point of the stimulus animal was approximately 0.5 cm away from the nose point of the recording animal. Four stimuli were presented to the recording mouse: a sexually experienced adult male mouse, a adult female mouse, a male juvenile and a mouse-shaped cotton toy. Each stimulus was presented for 10 seconds, with 50 seconds interval, for 5 times. For each animal, the recording was performed when the female was in diestrus, estrus and lactation. The ΔF/F of all recording sessions of each animal was divided by the maximum ΔF/F across sessions of that animal to obtain the normalized ΔF/F ranging from 0 to 1. Male preference index was calculated as the peak ΔF/F during male presentation divided by the sum of all stimuli (male+female+juvenile). We recorded 10-s ultrasound vocalization (USV) at a sampling rate of 250 kHz when a male investigated a female and played the USV, either alone or together with the presentation of an anesthetized adult male, to the head-fixed recording female (Avisoft-RECORDER USGH). The speaker (Avisoft-UltraSoundGate 116H) was placed 2 cm away from the mouse ear. The anesthetized male, USV, and USV+ male were presented in an interleaved order for 10 times each. Each stimulus presentation lasted for 10 seconds, with 50 seconds in between. Given that the Ca^{2+} response during the first male presentation was typically much higher than the rest, we introduced the male for an extra time prior to the 10 repeats, i.e. male was presented for 11 times, and excluded the first male presentation from the final analysis.

Slice electrophysiology—Female $Cckar^{Cre}$;Ai9;$Esr1^{ZsGreen}$ triple heterozygote mice were used for *in vitro* slice electrophysiological recording. Before slice preparation, the estrous state of the female was determined based on vaginal smear. Then, the mice were anesthetized with isoflurane, underwent transcardial perfusion with 20 ml ice-cold cutting solution containing (in mM): 110 choline chloride, 25 NaHCO3, 2.5 KCl, 7 MgCl2, 0.5 CaCl2, 1.25 NaH2PO4, 25 glucose, 11.6 ascorbic acid and 3.1 pyruvic acid. Brains were removed and submerged in ice-cold cutting solution, coronal sections of 275 μm at the level of VMH were cut on a Leica VT1200s vibratome and incubated in artificial cerebral spinal fluid (ACSF) containing (in mM): 125 NaCl, 2.5 KCl, 1.25 NaH2PO4, 25 NaHCO3, 1 MgCl2, 2 CaCl2 and 11 glucoses at 34°C for 30 min and then transferred to room temperature for cell recovery until the start of recording.

The recorded cells were visualized using an upright microscope (Olympus BX51WI) and were deemed to be within the VMHvll. The cells expressed either both ZsGreen and tdTomato ($VMHvll^{Cckar+Esr1+}$) or ZsGreen but not tdTomato ($VMHvll^{Cckar-Esr1+}$). All recordings were acquired from the dense Cckar+Esr1+ cluster in the VMHvll between Bregma level −1.70 to −1.94 mm. The $VMHvll^{Cckar-Esr1+}$ were intermingled with $VMHvll^{Cckar+Esr1+}$ cells. Of note, since virtually all VMHvll tdTomato expressing cells are ZsGreen positive, $VMHvll^{Cckar}$ cells are equivalent to $VMHvll^{Cckar+Esr1+}$ cells. To explore

cell firing properties, cell-attached and whole-cell patch-clamp current clamp recordings were made using glass electrodes (2–5 MΩ) containing (in mM): 145 K-gluconate, 2 MgCl2, 2 Na2ATP, 10 HEPES, 0.2 EGTA (286 mOsm, pH 7.2) without changing the pipette (Chieng et al., 2011). Upon gigaseal formation, the cell was held at −70 mV and data acquisition started, typically within one minute after completing cell-attached recording. For whole-cell mode, the action potential frequency was measured by calculating the number of the action potentials in a 500-ms-long depolarizing current step in current-clamp mode. The current step consisted of a series of sweeps from −20 pA to 500 pA, with a 20 pA step. The resting membrane potential was defined as membrane potential measured when no current was injected and within 30 seconds after membrane break in. Input resistance was determined by applying a small negative current step, presumably eliciting no or very limited opening of voltage-gated ion channels and dividing the measured ΔV by the injected current. We excluded 4 $VMHvll^{Cckar+Esr1+}$ cells in estrus and 6 $VMHvll^{Cckar-Esr1+}$ cells in estrus, 4 $VMHvll^{Cckar-Esr1+}$ cells in diestrus, and 4 $VMHvll^{Cckar-Esr1+}$ cells in lactation in Figure S16, due to the high spontaneous firing of those cells.

The whole-cell voltage recording of sEPSCs and sIPSCs was made using glass electrodes containing (in mM): 135 CsMeSO3, 10 HEPES, 1 EGTA, 3.3 QX-314 (chloride salt), 4 Mg-ATP, 0.3 Na-GTP and 8 sodium phosphocreatine (pH 7.3 adjusted with CsOH). sEPSCs were sampled at the reversal potential of Cl- (Vhold = −70 mV) and sIPSCs were sampled at the reversal potential of fast excitatory neurotransmission (Vhold = 0 mV). To quantify the frequency and amplitude of sEPSCs and sIPSCs, we measured all the peaks and its preceding troughs with custom written Matlab code, and using the peak time to represent the time of each event and the difference between the peak and its preceding trough as its amplitude. Traces were low pass filtered at 2 kHz, and the baseline was adjusted to be flat in Clampfit before analysis, the threshold for event detection was 5 pA for sEPSCs and 10 pA for sIPSCs.

Series resistance (less than 20 MΩ) was compensated by 80% and monitored periodically during the experiment with Multiclamp 700B amplifier (Molecular Devices, Sunnyvale, CA, USA). Signals were recorded using MultiClamp 700B amplifier, digitized by DigiData1550B with a sampling rate of 20 kHz (Molecular Devices, USA). Electrophysiological data were analyzed using Clampfit (Molecular Devices, RRID:SCR_011323) or Matlab (Mathworks, RRID:SCR_001622).

QUANTIFICATION AND STATISTICAL ANALYSIS

All plots and graphs were edited in Adobe Illustrator (Adobe, RRID:SCR_010279) for the final publication. All statistical analysis were performed using MATLAB (Mathworks, RRID:SCR_001622) or Prism 9 (GraphPad Software, RRID:SCR_002798). All statistical analyses were two-tailed. If there were missing values, a mixed-effects model was implemented. Parametric tests, including paired t test, unpaired t test and One-way ANOVA were used if distributions passed Shapiro-Wilk tests for normality (except One-way ANOVA with missing values and Two-way ANOVA, which data distribution was assumed to be normal, but was not formally tested), or else a nonparametric test was used if distributions were not normally distributed. Statistical significance between two groups was determined

using paired or unpaired student's t test based on whether the data were paired or not. Difference between one group and a hypothetical value was determined using one sample test (normal data) or one sample Wilcoxon signed-rank test (non-normal data). For more than two groups repeated tests, statistical significances were determined using RM One-way ANOVA followed with Tukey's multiple comparisons test (normal data) or Friedman test with Dunn's multiple comparisons test (non-normal data). For more than two independent non-matching groups, statistical significances were determined using One-way ANOVA followed with Tukey's multiple comparisons test (normal data) or Kruskal-Wallis test with Dunn's multiple comparisons test (non-normal data). Differences between two groups were determined using Two-way ANOVA followed with Sidak's multiple comparisons test. Difference between more than two groups were determined using Two-way ANOVA followed with Tukey's multiple comparisons test. All p values < 0.1 were indicated on the figures. *p< 0.05; **p<0.01; ***p<0.001; ****p<0.0001. For detailed number of animals or cells for each plot and statistical results, see Figure legends and Data S1.

Supplementary Material

Refer to Web version on PubMed Central for supplementary material.

Acknowledgments

We thank S.Y. Kim (NYULMC Rodent Genetic Engineering Laboratory) for assistance in generating the Cckar^{Cre} mouse, D.L.K. Tavakol (NYULMC) for demonstrating ovariectomy, B. Ruby (NYULMC) for providing Ai9 mice, Y. Xu (Baylor College of Medicine) for providing Esr1^{Zsgreen} mice, M. Vöröslakos and Z. Guo for advice on *in vivo* recording, and C. Haddaway and Y. Jiang for help with genotyping and behavioral testing. This research was supported by NIH grants R01MH101377, 1R01HD092596 and U19NS107616 (D.L.); the Mathers Foundation (D.L.); the Leon Levy Neuroscience Fellowship and NIMH K99MH127295 (J.E.L); the Uehara Memorial Foundation, JSPS Overseas Research Fellowship and Osamu Hayaishi Memorial Scholarship (T.O.).

References

Ajayi AF, and Akhigbe RE (2020). Staging of the estrous cycle and induction of estrus in experimental rodents: an update. Fertil Res Pract 6, 5. [PubMed: 32190339]

Andermann ML, and Lowell BB (2017). Toward a Wiring Diagram Understanding of Appetite Control. Neuron 95, 757–778. [PubMed: 28817798]

Armbruster BN, Li X, Pausch MH, Herlitze S, and Roth BL (2007). Evolving the lock to fit the key to create a family of G protein-coupled receptors potently activated by an inert ligand. 104, 5163–5168.

Babcock AM, Bloch GJ, and Micevych PE (1988). Injections of cholecystokinin into the ventromedial hypothalamic nucleus inhibit lordosis behavior in the rat. Physiology behavior 43, 195–199. [PubMed: 3212055]

Beach FA (1976). Sexual attractivity, proceptivity, and receptivity in female mammals. Horm Behav 7, 105–138. [PubMed: 819345]

Berridge KC (2004). Motivation concepts in behavioral neuroscience. Physiol Behav 81, 179–209. [PubMed: 15159167]

Berrios J, Li C, Madara JC, Garfield AS, Steger JS, Krashes MJ, and Lowell BB (2021). Food cue regulation of AGRP hunger neurons guides learning. Nature 595, 695–700. [PubMed: 34262177]

Bloch GJ, Babcock AM, Gorski RA, and Micevych PE (1987). Cholecystokinin stimulates and inhibits lordosis behavior in female rats. Physiol Behav 39, 217–224. [PubMed: 3575456]

Burnett CJ, Li C, Webber E, Tsaousidou E, Xue SY, Bruning JC, and Krashes MJ (2016). Hunger-Driven Motivational State Competition. Neuron 92, 187–201. [PubMed: 27693254]

Calizo LH, and Flanagan-Cato LM (2000). Estrogen selectively regulates spine density within the dendritic arbor of rat ventromedial hypothalamic neurons. J Neurosci 20, 1589–1596. [PubMed: 10662848]

Canteras NS, Simerly RB, and Swanson LW (1995). Organization of projections from the medial nucleus of the amygdala: a PHAL study in the rat. J Comp Neurol 360, 213–245. [PubMed: 8522644]

Chen TW, Wardill TJ, Sun Y, Pulver SR, Renninger SL, Baohan A, Schreiter ER, Kerr RA, Orger MB, Jayaraman V, et al. (2013). Ultrasensitive fluorescent proteins for imaging neuronal activity. Nature 499, 295–300. [PubMed: 23868258]

Chieng B, Azriel Y, Mohammadi S, and Christie MJ (2011). Distinct cellular properties of identified dopaminergic and GABAergic neurons in the mouse ventral tegmental area. J Physiol 589, 3775–3787. [PubMed: 21646409]

Cottingham SL, Femano PA, and Pfaff DW (1987). Electrical stimulation of the midbrain central gray facilitates reticulospinal activation of axial muscle EMG. Exp Neurol 97, 704–724. [PubMed: 3622719]

Dey S, Chamero P, Pru JK, Chien MS, Ibarra-Soria X, Spencer KR, Logan DW, Matsunami H, Peluso JJ, and Stowers L (2015). Cyclic Regulation of Sensory Perception by a Female Hormone Alters Behavior. Cell 161, 1334–1344. [PubMed: 26046438]

Dong HW, and Swanson LW (2004). Projections from bed nuclei of the stria terminalis, posterior division: implications for cerebral hemisphere regulation of defensive and reproductive behaviors. J Comp Neurol 471, 396–433. [PubMed: 15022261]

Dornan WA, Bloch GJ, Priest CA, and Micevych PE (1989). Microinjection of cholecystokinin into the medial preoptic nucleus facilitates lordosis behavior in the female rat. Physiology behavior 45, 969–974. [PubMed: 2780882]

Eliasson M, and Meyerson BJ (1975). Sexual preference in female rats during estrous cycle, pregnancy and lactation. Physiol Behav 14, 705–710. [PubMed: 1237902]

Falkner AL, Grosenick L, Davidson TJ, Deisseroth K, and Lin D (2016). Hypothalamic control of male aggression-seeking behavior. Nature neuroscience 19, 596–604. [PubMed: 26950005]

Frankfurt M, Siegel RA, Sim I, and Wuttke W (1986). Estrous Cycle Variations in Cholecystokinin and Substance P Concentrations in Discrete Areas of the Rat Brain. Neuroendocrinology 42, 226–231. [PubMed: 2419781]

Gandelman R (1972). Mice: postpartum aggression elicited by the presence of an intruder. Hormones Behavior 3, 23–28. [PubMed: 4681734]

Gorski RA (1976). The possible neural sites of hormonal facilitation of sexual behavior in the female rat. Psychoneuroendocrinology 1, 371–387.

Goy RW, and Phoenix CH (1963). Hypothalamic regulation of female sexual behaviour; establishment of behavioural oestrus in spayed guinea-pigs following hypothalamic lesions. J Reprod Fertil 5, 23–40. [PubMed: 13949643]

Green JA (1978). Experiential determinants of postpartum aggression in mice. J Comp Physiol Psychol 92, 1179–1187. [PubMed: 573286]

Hardy DF (1972). Sexual behavior in continuously cycling rats. Behaviour 41, 288–297. [PubMed: 5063409]

Hashikawa K, Hashikawa Y, Tremblay R, Zhang J, Feng JE, Sabol A, Piper WT, Lee H, Rudy B, and Lin D (2017a). Esr1(+) cells in the ventromedial hypothalamus control female aggression. Nature neuroscience 20, 1580–1590. [PubMed: 28920934]

Hashikawa Y, Hashikawa K, Falkner AL, and Lin D (2017b). Ventromedial Hypothalamus and the Generation of Aggression. Front Syst Neurosci 11, 94. [PubMed: 29375329]

Hayashi S, and Kimura T (1974). Sex-attractant emitted by female mice. Physiol Behav 13, 563–567. [PubMed: 4475431]

Hellier V, Brock O, and Bakker J (2019). The Role of Kisspeptin in Sexual Behavior. Semin Reprod Med 37, 84–92. [PubMed: 31847028]

Inoue S (2021). Neural basis for estrous cycle-dependent control of female behaviors. Neurosci Res.

Inoue S, Yang R, Tantry A, Davis CH, Yang T, Knoedler JR, Wei Y, Adams EL, Thombare S, Golf SR, et al. (2019). Periodic Remodeling in a Neural Circuit Governs Timing of Female Sexual Behavior. Cell 179, 1393–1408 e1316. [PubMed: 31735496]

Jennings KJ, and de Lecea L (2020). Neural and Hormonal Control of Sexual Behavior. Endocrinology 161.

Kaidanovich-Beilin O, Lipina T, Vukobradovic I, Roder J, and Woodgett JR (2011). Assessment of social interaction behaviors. J Vis Exp.

Kavaliers M, Wiebe JP, and Galea L.A.J.B.r. (1994). Male preference for the odors of estrous female mice is enhanced by the neurosteroid 3α-hydroxy-4-pregnen-20-one (3αHP). Brain Res 646, 140–144. [PubMed: 8055331]

Kendrick AM, Rand MS, and Crews D (1995). Electrolytic lesions to the ventromedial hypothalamus abolish receptivity in female whiptail lizards, Cnemidophorus uniparens. Brain Res 680, 226–228. [PubMed: 7663980]

Kim CK, Yang SJ, Pichamoorthy N, Young NP, Kauvar I, Jennings JH, Lerner TN, Berndt A, Lee SY, Ramakrishnan C, et al. (2016). Simultaneous fast measurement of circuit dynamics at multiple sites across the mammalian brain. Nat Methods 13, 325–328. [PubMed: 26878381]

Kim DW, Yao Z, Graybuck LT, Kim TK, Nguyen TN, Smith KA, Fong O, Yi L, Koulena N, Pierson N, et al. (2019). Multimodal Analysis of Cell Types in a Hypothalamic Node Controlling Social Behavior. Cell 179, 713–728 e717. [PubMed: 31626771]

Knoedler JR, Inoue S, Bayless DW, Yang T, Tantry A, Davis C. h., Leung NY, Parthasarathy S, Wang G, Alvarado M, et al. (2022). A functional cellular framework for sex and estrous cycle-dependent gene expression and behavior. Cell Online.

Kow LM, and Pfaff DW (1986). CCK-8 stimulation of ventromedial hypothalamic neurons in vitro: a feeding-relevant event? Peptides 7, 473–479. [PubMed: 3774589]

Krashes MJ, Koda S, Ye C, Rogan SC, Adams AC, Cusher DS, Maratos-Flier E, Roth BL, and Lowell BB (2011). Rapid, reversible activation of AgRP neurons drives feeding behavior in mice. J Clin Invest 121, 1424–1428. [PubMed: 21364278]

Le Moene O, Hernandez-Arteaga E, Chu X, and Agmo A (2020). Rapid changes in sociosexual behaviors around transition to and from behavioral estrus, in female rats housed in a seminatural environment. Behav Processes 174, 104101. [PubMed: 32119907]

Leedy MG, and Hart BL (1985). Female and male sexual responses in female cats with ventromedial hypothalamic lesions. Behav Neurosci 99, 936–941. [PubMed: 3843309]

Lenschow C, and Lima SQ (2020). In the mood for sex: neural circuits for reproduction. Curr Opin Neurobiol 60, 155–168. [PubMed: 31901622]

Lin D, Boyle MP, Dollar P, Lee H, Lein ES, Perona P, and Anderson DJ (2011). Functional identification of an aggression locus in the mouse hypothalamus. Nature 470, 221–226. 10.1038/nature09736. [PubMed: 21307935]

Liu M, Kim D-W, Zeng H, and Anderson D (2022). Make war not love: The neural substrate underlying a state-dependent switch in female social behavior. Neuron.

Liu Q, Yang D, Zhuang Y, Croll TI, Cai X, Dai A, He X, Duan J, Yin W, Ye C, et al. (2021). Ligand recognition and G-protein coupling selectivity of cholecystokinin A receptor. Nature Chemical Biology 17, 1238–1244. [PubMed: 34556862]

Livneh Y, Ramesh RN, Burgess CR, Levandowski KM, Madara JC, Fenselau H, Goldey GJ, Diaz VE, Jikomes N, Resch JM, et al. (2017). Homeostatic circuits selectively gate food cue responses in insular cortex. Nature 546, 611–616. [PubMed: 28614299]

Madeira MD, Ferreira-Silva L, and Paula-Barbosa MM (2001). Influence of sex and estrus cycle on the sexual dimorphisms of the hypothalamic ventromedial nucleus: stereological evaluation and Golgi study. J Comp Neurol 432, 329–345. [PubMed: 11246211]

Madisen L, Zwingman TA, Sunkin SM, Oh SW, Zariwala HA, Gu H, Ng LL, Palmiter RD, Hawrylycz MJ, Jones AR, et al. (2010). A robust and high-throughput Cre reporting and characterization system for the whole mouse brain. Nature neuroscience 13, 133–140. [PubMed: 20023653]

Mahn M, Gibor L, Patil P, Cohen-Kashi Malina K, Oring S, Printz Y, Levy R, Lampl I, and Yizhar O (2018). High-efficiency optogenetic silencing with soma-targeted anion-conducting channelrhodopsins. Nat Commun 9, 4125. [PubMed: 30297821]

Martinez de Morentin PB, Gonzalez-Garcia I, Martins L, Lage R, Fernandez-Mallo D, Martinez-Sanchez N, Ruiz-Pino F, Liu J, Morgan DA, Pinilla L, et al. (2014). Estradiol regulates brown adipose tissue thermogenesis via hypothalamic AMPK. Cell Metab 20, 41–53. [PubMed: 24856932]

Mathews D, Donovan KM, Hollingsworth EM, Hutson VB, and Overstreet CT (1983). Permanent deficits in lordosis behavior in female rats with lesions of the ventromedial nucleus of the hypothalamus. Exp Neurol 79, 714–719. [PubMed: 6825760]

McCarthy EA, Naik AS, Coyne AF, Cherry JA, and Baum MJ (2018). Effect of Ovarian Hormones and Mating Experience on the Preference of Female Mice to Investigate Male Urinary Pheromones. Chem Senses 43, 97–104. [PubMed: 29211837]

Micevych P, Akesson T, and Elde R (1988). Distribution of cholecystokinin-immunoreactive cell bodies in the male and female rat: II. Bed nucleus of the stria terminalis and amygdala. J Comp Neurol 269, 381–391. [PubMed: 3372720]

Micevych PE, and Meisel RL (2017). Integrating Neural Circuits Controlling Female Sexual Behavior. Front Syst Neurosci 11, 42. [PubMed: 28642689]

Miller NE (1971). Neal E. Miller: selected papers (Chicago,: Aldine).

Miura H, Quadros RM, Gurumurthy CB, and Ohtsuka M (2018). Easi-CRISPR for creating knock-in and conditional knockout mouse models using long ssDNA donors. Nature protocols 13, 195–215. [PubMed: 29266098]

Musatov S, Chen W, Pfaff DW, Kaplitt MG, and Ogawa S (2006). RNAi-mediated silencing of estrogen receptor {alpha} in the ventromedial nucleus of hypothalamus abolishes female sexual behaviors. Proc Natl Acad Sci U S A 103, 10456–10460. [PubMed: 16803960]

Nomoto K, and Lima Susana Q. (2015). Enhanced Male-Evoked Responses in the Ventromedial Hypothalamus of Sexually Receptive Female Mice. Current Biology 25, 589–594. [PubMed: 25683805]

Oh SW, Harris JA, Ng L, Winslow B, Cain N, Mihalas S, Wang Q, Lau C, Kuan L, Henry AM, et al. (2014). A mesoscale connectome of the mouse brain. Nature 508, 207–214. 10.1038/nature13186. [PubMed: 24695228]

Oro AE, Simerly RB, and Swanson LW (1988). Estrous cycle variations in levels of cholecystokinin immunoreactivity within cells of three interconnected sexually dimorphic forebrain nuclei. Evidence for a regulatory role for estrogen. Neuroendocrinology 47 3, 225–235. [PubMed: 3362304]

Osborne JE, and Dudman JT (2014). RIVETS: a mechanical system for in vivo and in vitro electrophysiology and imaging. PLoS One 9, e89007. [PubMed: 24551206]

Pfaff DW, and Sakuma Y (1979). Facilitation of the lordosis reflex of female rats from the ventromedial nucleus of the hypothalamus. J Physiol 288, 189–202. [PubMed: 469715]

Pomerantz SM, Nunez AA, and Bean NJ (1983). Female behavior is affected by male ultrasonic vocalizations in house mice. Physiology behavior 31, 91–96. [PubMed: 6685321]

Robarts DW, and Baum MJ (2007). Ventromedial hypothalamic nucleus lesions disrupt olfactory mate recognition and receptivity in female ferrets. Horm Behav 51, 104–113. [PubMed: 17011561]

Saito K, He Y, Yan X, Yang Y, Wang C, Xu P, Hinton AO Jr., Shu G, Yu L, Tong Q, et al. (2016). Visualizing estrogen receptor-alpha-expressing neurons using a new ERalpha-ZsGreen reporter mouse line. Metabolism 65, 522–532. [PubMed: 26975544]

Sakuma Y, and Pfaff DW (1979a). Facilitation of female reproductive behavior from mesensephalic central gray in the rat. Am J Physiol 237, R278–284. [PubMed: 495775]

Sakuma Y, and Pfaff DW (1979b). Mesencephalic mechanisms for integration of female reproductive behavior in the rat. Am J Physiol 237, R285–290. [PubMed: 495776]

Sales GD (1972). Ultrasound and mating behaviour in rodents with some observations on other behavioural situations. Journal of Zoology 168, 149–164.

Sanchez-Alavez M, Alboni S, and Conti B (2011). Sex- and age-specific differences in core body temperature of C57Bl/6 mice. Age (Dordr) 33, 89–99. [PubMed: 20635153]

Shao Y-Q, Fan L, Wu W-Y, Zhu Y-J, and Xu H-T (2022). A developmental switch between electrical and neuropeptide communication in the ventromedial hypothalamus. Current Biology.

Shelley DN, Choleris E, Kavaliers M, and Pfaff DW (2006). Mechanisms underlying sexual and affiliative behaviors of mice: relation to generalized CNS arousal. Soc Cogn Affect Neurosci 1, 260–270. [PubMed: 18985112]

Sternson SM, Nicholas Betley J, and Cao ZF (2013). Neural circuits and motivational processes for hunger. Curr Opin Neurobiol 23, 353–360. [PubMed: 23648085]

Sych Y, Chernysheva M, Sumanovski LT, and Helmchen F (2019). High-density multi-fiber photometry for studying large-scale brain circuit dynamics. Nat Methods 16, 553–560. [PubMed: 31086339]

van Veen JE, Kammel LG, Bunda PC, Shum M, Reid MS, Massa MG, Arneson D, Park JW, Zhang Z, Joseph AM, et al. (2020). Hypothalamic estrogen receptor alpha establishes a sexually dimorphic regulatory node of energy expenditure. Nat Metab 2, 351–363. [PubMed: 32377634]

Wang F, Flanagan J, Su N, Wang LC, Bui S, Nielson A, Wu X, Vo HT, Ma XJ, and Luo Y (2012). RNAscope: a novel in situ RNA analysis platform for formalin-fixed, paraffin-embedded tissues. J Mol Diagn 14, 22–29. [PubMed: 22166544]

Xu X, Coats Jennifer K., Yang Cindy F., Wang A, Ahmed Osama M., Alvarado M, Izumi T, and Shah Nirao M. (2012). Modular Genetic Control of Sexually Dimorphic Behaviors. Cell 148, 1066–1067.

Yang CF, Chiang MC, Gray DC, Prabhakaran M, Alvarado M, Juntti SA, Unger EK, Wells JA, and Shah NM (2013). Sexually dimorphic neurons in the ventromedial hypothalamus govern mating in both sexes and aggression in males. Cell 153, 896–909. [PubMed: 23663785]

Zhao Z-D, Yang WZ, Gao C, Fu X, Zhang W, Zhou Q, Chen W, Ni X, Lin J-K, Yang J, et al. (2017). A hypothalamic circuit that controls body temperature. Proc Natl Acad Sci U S A 114, 2042–2047. [PubMed: 28053227]

Zimmerman CA, and Knight ZA (2020). Layers of signals that regulate appetite. Current opinion in eurobiology 64, 79–88.

Highlights

- Inactivation of VMHvll^{Cckar} suppresses female sexual proceptivity and receptivity.
- Activation of VMHvll^{Cckar} promotes female sexual proceptivity and receptivity.
- VMHvll^{Cckar} is activated specifically by males and during female sexual behaviors.
- Physiological properties of VMHvll^{Cckar} cells change over reproductive cycle.

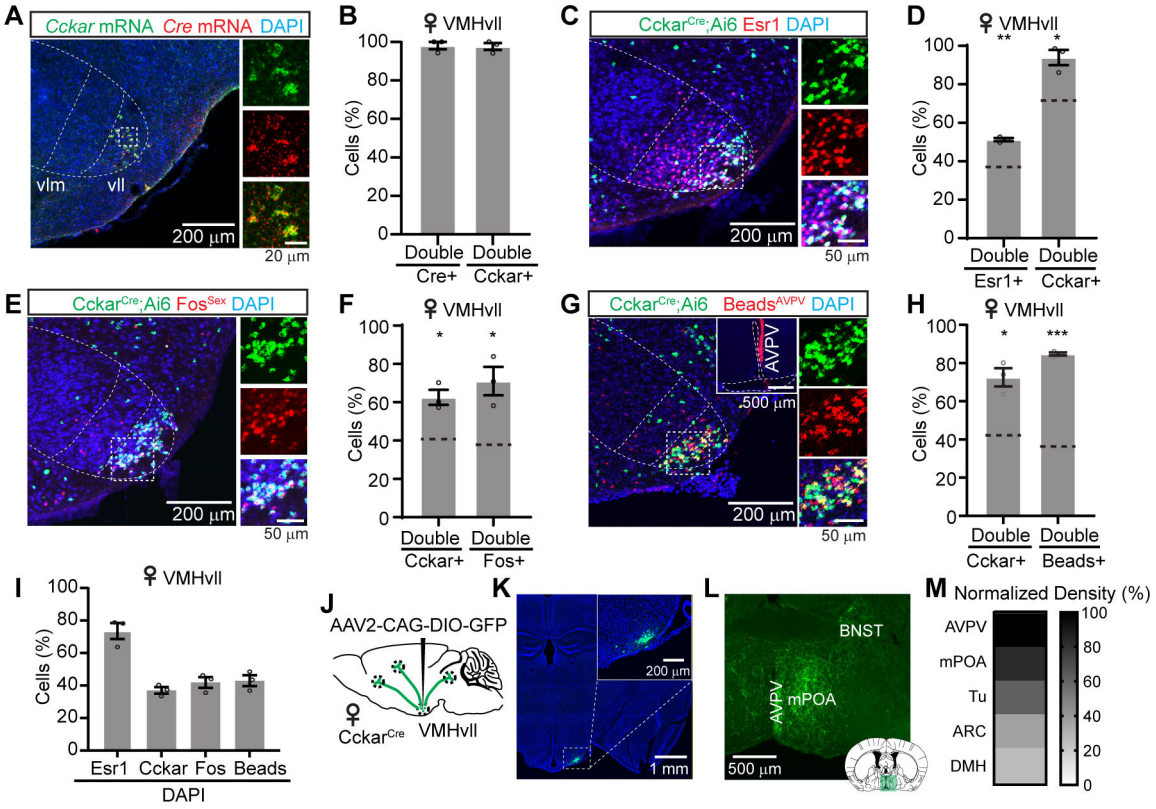

Figure 1. Characterization of VMHvll^{Cckar} cells

(A) *Cckar* and *Cre* mRNA in the VMHvl of a Cckar^{Cre} female mouse.

(B) Overlap between VMHvll *Cre* and *Cckar* mRNA.

(C) Esr1 staining in the VMHvl of a Cckar^{Cre};Ai6 female mouse.

(D) Overlap between VMHvll Esr1 and Cckar.

(E) Immunostaining of sexual behavior induced Fos (Fos^{Sex}) in the VMHvl of a Cckar^{Cre};Ai6 female mouse.

(F) Overlap between VMHvll Cckar and Fos^{Sex}.

(G) Retrobead-labeled VMHvll cells from AVPV of a Cckar^{Cre};Ai6 female mouse. Insert shows injection site.

(H) Overlap between Cckar and retrobead cells in VMHvll.

(I) The percentage of Esr1, Cckar, Fos^{Sex} and retrobeads cells in VMHvll in DAPI+ cells.

(J) Viral strategy for axon tracing of VMHvll^{Cckar} cells.

(K) GFP expression in the VMHvll^{Ccka} cells. Inset, the zoom-in view of the boxed area.

(L) GFP expressing terminals from VMHvll^{Cckar} at AVPV, BNST and mPOA.

(M) The top five brain regions that receive inputs from VMHvll^{Cckar}.

In (A, C, E, G), right shows the enlarged view of the boxed area. Dotted lines demarcate VMH subdivisions. In (D, F, H), horizontal dashed lines indicate the chance level of overlap. Data are mean ± s.e.m. (D, F, H) One sample t test. *p<0.05; **p<0.01; ***p<0.001. n = 3 animals (B, D, F, H, I, M).

See also Figures S1–S3.

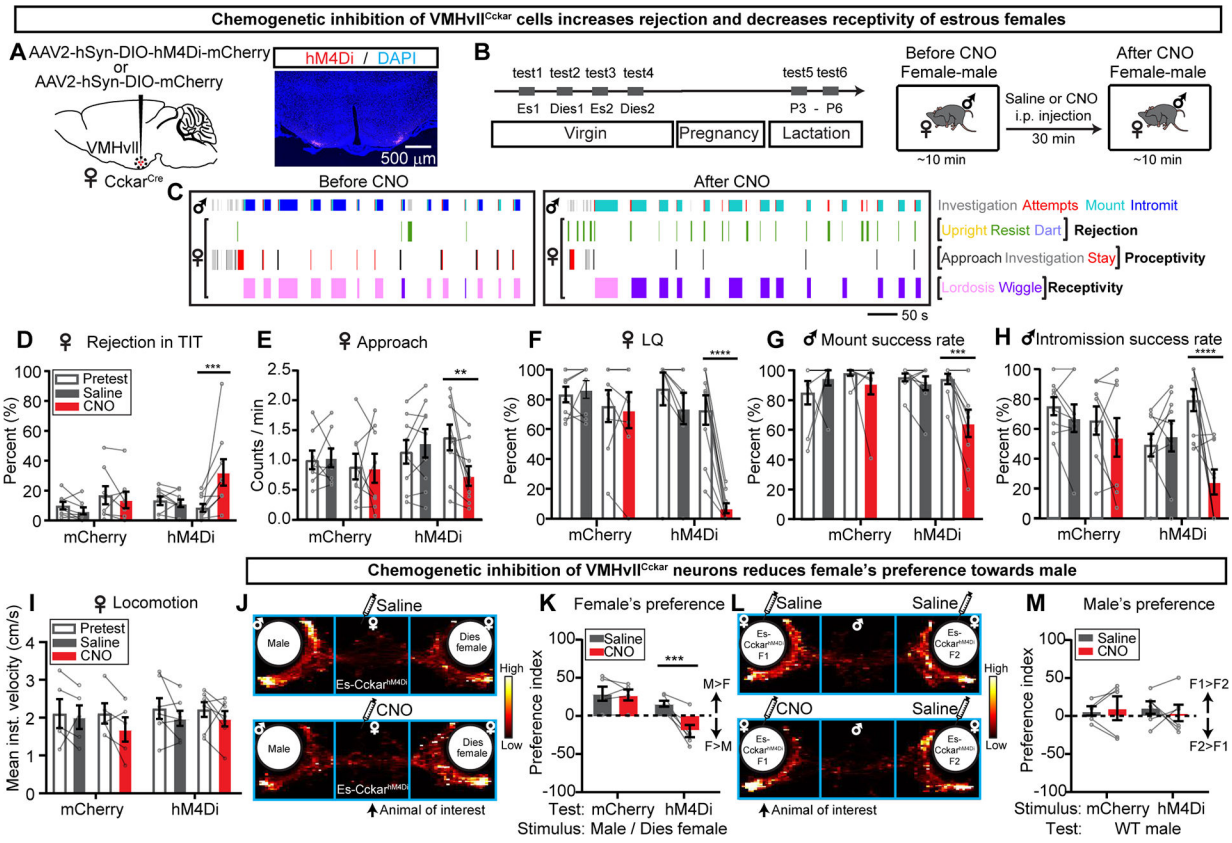

Figure 2. Chemogenetic inhibition of VMHvll^{Cckar} cells suppresses female sexual behaviors

(A) Viral strategy and histology.

(B) Experimental timeline.

(C) Behavior raster plots of a male and an estrous Cckar^{hM4Di} female before and after CNO injection to the female.

(D-I) Percentage of time female spent on rejecting the male (summation of upright, resist and dart) during total interaction time (D), frequency of approach initiated by females (E), lordosis quotient (LQ) (F), male mount success rate (G), male intromission success rate (H), average locomotion velocity of solitary females calculated over 30 minutes (I) before and after saline or CNO injection.

(J) The distribution of female's body center location after saline or CNO injection.

(K) Test female's preference index (PI). Positive values indicate male preference.

(L) The distribution of the male's body center location. The stimulus animals are injected either both with saline (top) or one with CNO and one with saline (bottom).

(M) Comparison of male's preference index. Positive values indicate preference of CNO injected females.

Data are mean ± s.e.m. (D-I, K, M) Two-way ANOVA followed by Sidak's multiple comparisons test. **p<0.01; ***p<0.001; ****p<0.0001.

n = number of animals. mCherry: n=8 (D-H), 5 (I, K, M); hM4Di: n=9 (D-H), 7 (I), 6 (K, M).

See also Figures S4–S8.

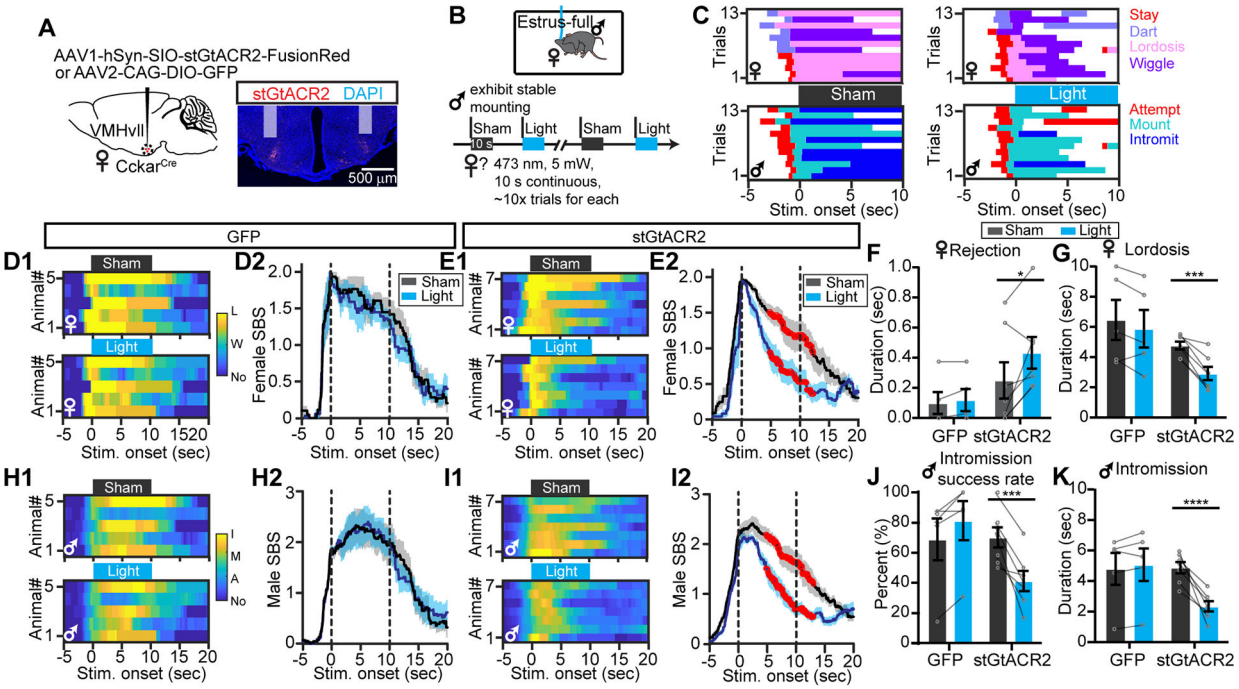

Figure 3. Optogenetic inhibition of VMHvll^{Cckar} cells impairs female sexual receptivity

(A) Viral strategy and histology. Shades indicate optic fiber tracks.

(B) Behavioral paradigm and stimulation protocol.

(C) Behavior raster plots of a female (top) and its paired male (bottom) during sham and light trials.

(D) Heatmaps (D1) and PSTHs (D2) showing female SBS aligned to sham or light onset of all Cckar^{GFP} females. L: lordosis; W: wiggle: No: no mating.

(E) Same as (D), but for all Cckar^{stGtACR2} females.

(F and G) The average duration females spent on rejecting the male (F) and lordosis (G) during sham and light stimulation of Cckar^{GFP} and Cckar^{stGtACR2} females.

(H-I) Male SBS aligned to the onsets of sham or light stimulation delivered to the paired Cckar^{GFP} (H) or Cckar^{stGtACR2} females (I). I: intromission; M: mount: A: attempt to mount; No: no mating.

(J and K) Male intromission success rate (J) and the average male intromission duration (K) during sham and light trials when the male was paired with Cckar^{GFP} or Cckar^{stGtACR2} females.

Data are mean ± s.e.m. (D2, E2, H2, I2) Two-way ANOVA with repeated measures, followed by Sidak's multiple comparisons test. Red dots indicate periods when SBS differ significantly ($p<0.05$) between sham and light trials. Dashes vertical lines indicate sham and light periods. (F, G, J, K) Two-way ANOVA followed by Sidak's multiple comparisons test. *$p<0.05$; ***$p<0.001$; ****$p<0.0001$.

n = 5 animals for GFP group, and 7 for stGtACR2 group.

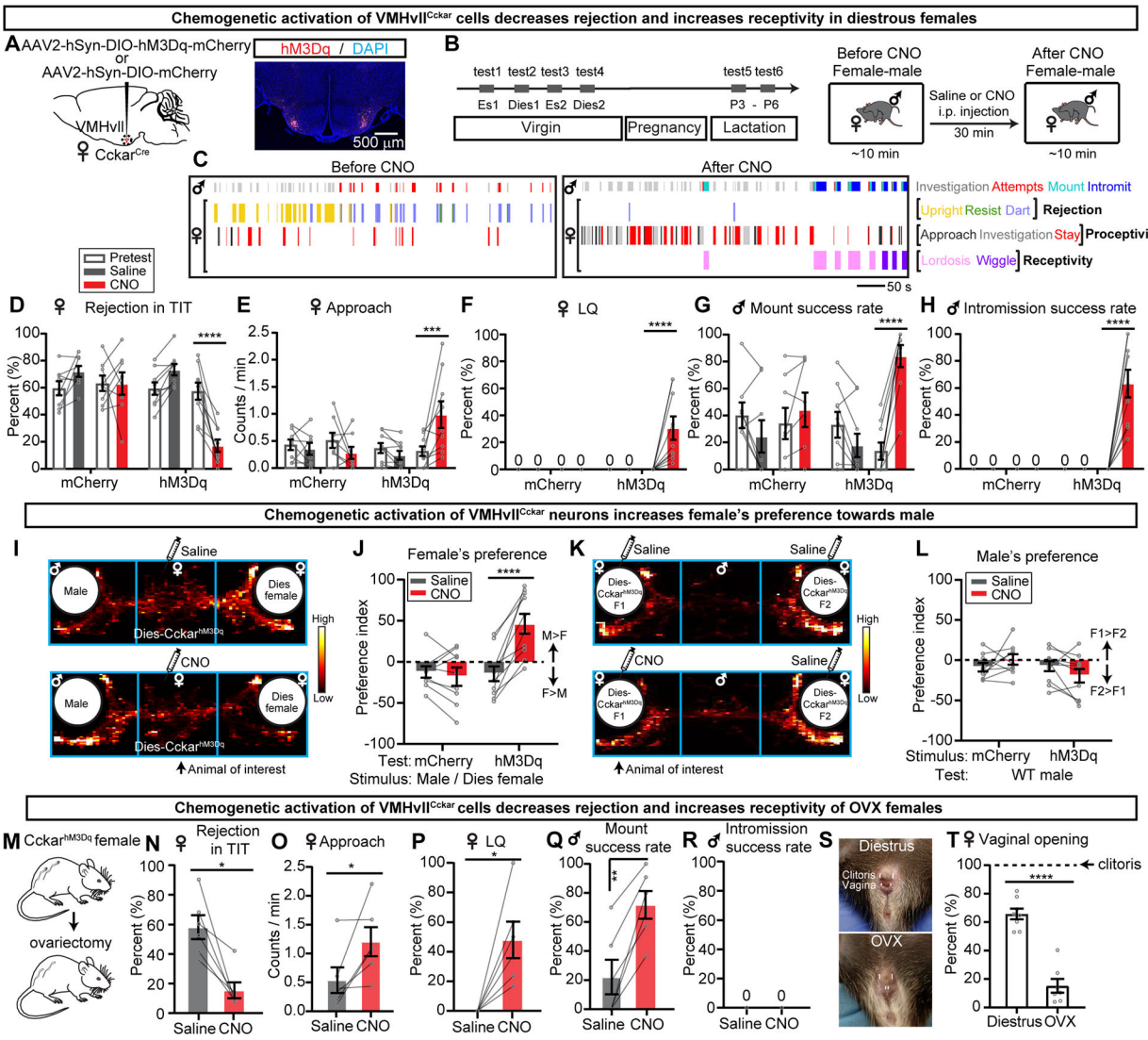

Figure 4. Chemogenetic activation of VMHvll^{Cckar} cells promotes female proceptivity and receptivity

(A) Viral strategy and histology.

(B) Experimental timeline.

(C) Behavior raster plots of a male and a diestrous Cckar^{hM3Dq} female before and after CNO injection to females.

(D-H) Percentage of time female spent on rejecting the male (D), frequency of female initiated approach (E), LQ (F), male mount success rate (G), male intromission success rate (H) before and after saline or CNO injection.

(I) Distribution of female's body center location before and after saline or CNO.

(J) Female's PI. Positive values indicate male preference.

(K) Distribution of a male's body center location.

(L) Male's PI. Positive values indicate preference for CNO-injected female.

(M) Ovariectomy.

(N-R) Percentage of time female spent on rejecting the male (N), female-initiated approaches frequency (O), LQ (P), male mount success rate (Q), male intromission success rate (R) before and after saline or CNO injection to females.
(S) Female vaginal opening in diestrous and OVX females. Upper and lower short lines denote clitoris and vaginal opening, respectively.
(T) Width of female vaginal opening normalized to that of clitoris in diestrous and OVX females.
Data are mean ± s.e.m. (D-H, J, L) Two-way ANOVA followed by Sidak's multiple comparisons test. (N-O) Two-tailed Wilcoxon matched-pairs signed rank test. (P) One-sample t test, with hypothetical value as 0. (Q) Two-tailed paired t test. (T) Two-tailed unpaired t test. *p<0.05; **p<0.01; ***p<0.001; ****p<0.0001.
n = number of animals. n=8 (D-H) and 9 (J, L) mCherry females; n=9 (D-H) and n=10 (J, L) hM3Dq females; n=6 (N-R) OVX-hM3Dq females; n=8 (T) for diestrous and n=7 (T) for OVX-hM3Dq females.
See also Figures S4, S5, S8–S10.

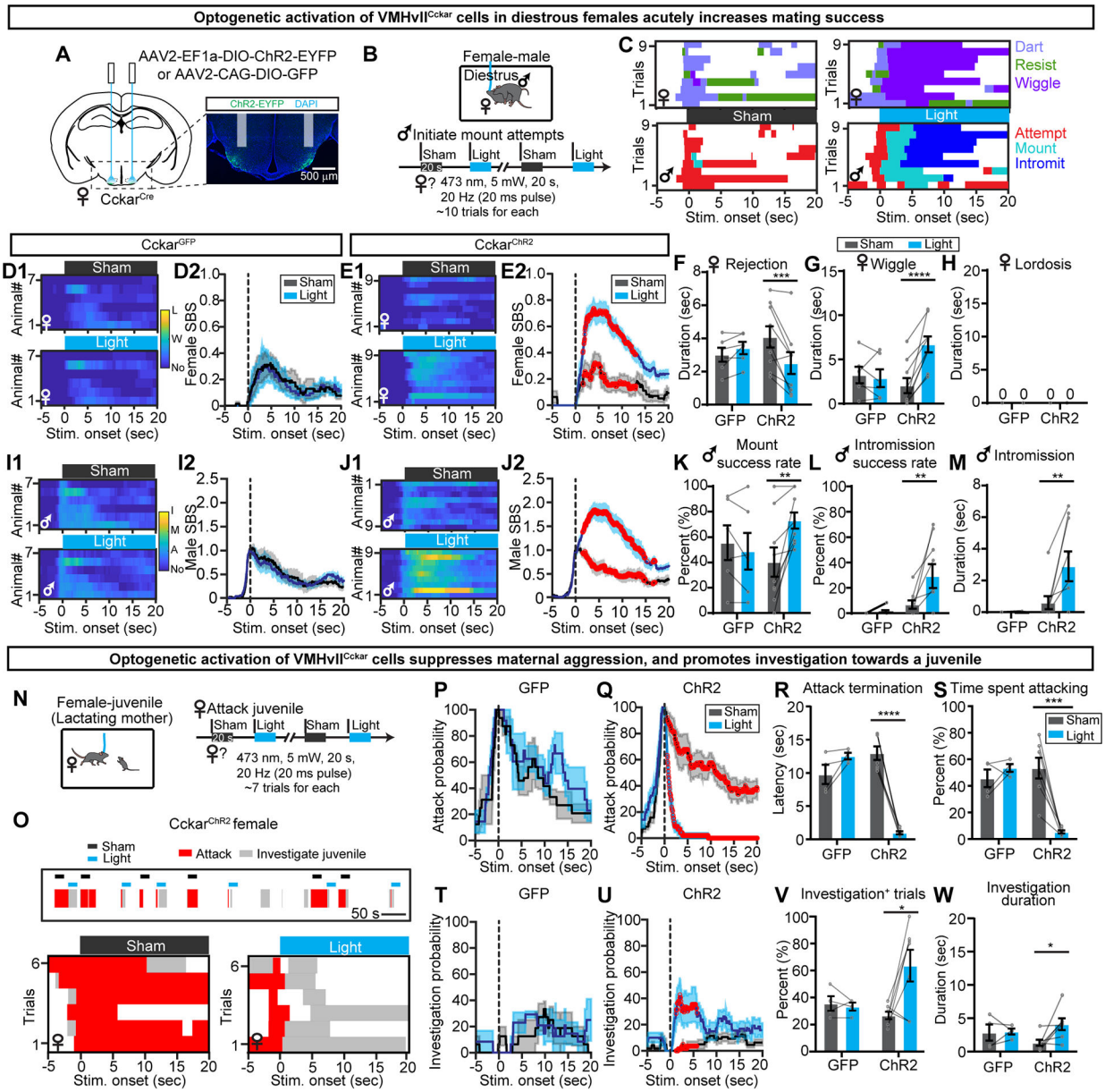

Figure 5. Optogenetic activation of VMHvll^{Cckar} cells increases mating success and suppresses maternal aggression in females

(A) Viral strategy and histology. Shades indicate optic fiber tracks.

(B) Behavioral paradigm and stimulation protocol.

(C) Behavior raster plots of a female (top) and its paired male (bottom) during sham and light stimulation of the female.

(D) Heatmaps (D1) and PSTHs (D2) showing female SBS aligned to the onset of sham or light stimulation of all diestrous Cckar^{GFP} females. L: lordosis; W: wiggle: No: no mating.

(E) Same as (D), but for Cckar^{ChR2} females.

(F-H) The average duration females spent on rejecting the male (F), wiggle (G) and lordosis (H) during sham and light stimulation of Cckar^{GFP} and Cckar^{ChR2} females.

(I-J) Male SBS aligned to the onset of sham or light delivered to the paired $Cckar^{GFP}$ (I) or $Cckar^{ChR2}$ females. I: intromission; M: mount: A: attempt to mount; No: no mating.
(K-M) Male mount success rate (K), intromission success rate (L), and average male intromission duration (M) during sham and light trials when the male was paired with $Cckar^{GFP}$ or $Cckar^{ChR2}$ females.
(N) Behavioral paradigm and stimulation protocol. Stimulation started upon attack initiation.
(O) Behavior raster plots of a lactating $Cckar^{ChR2}$ female with a juvenile intruder upon sham and light simulation.
(P and Q) PSTHs of attack probability of lactating $Cckar^{GFP}$ (P) and $Cckar^{ChR2}$ (Q) females aligned to sham and light stimulation onset.
(R) The latency to terminate attack from the light or sham onset.
(S) The percent of time the females spent on attacking the juvenile during the sham and light periods.
(T and U) PSTHs of investigation probability of lactating $Cckar^{GFP}$ (T) and $Cckar^{ChR2}$ (U) females aligned to sham and light onset.
(V) Percentage of sham and light trials with female investigation of a juvenile.
(W) Juvenile investigation duration during sham and light trials.
Data are mean ± s.e.m. (D2, E2, I2, J2, P and Q, T and U) Two-way ANOVA with repeated measures, followed by Sidak's multiple comparisons test. Red dots indicate periods when SBS differ significantly ($p<0.05$) between sham and light trials. (F-G, K-M, R-S, V-W) Two-way ANOVA with Sidak's multiple comparisons test. *$p<0.05$; **$p<0.01$; ***$p<0.001$; ****$p<0.0001$;
n = number of animals. GFP: n=6 (D-M), 4 (P, R-S, T, V-W); ChR2: n=9 (D-M), 7 (Q, R-S, U, V-W).
See also Figure S11.

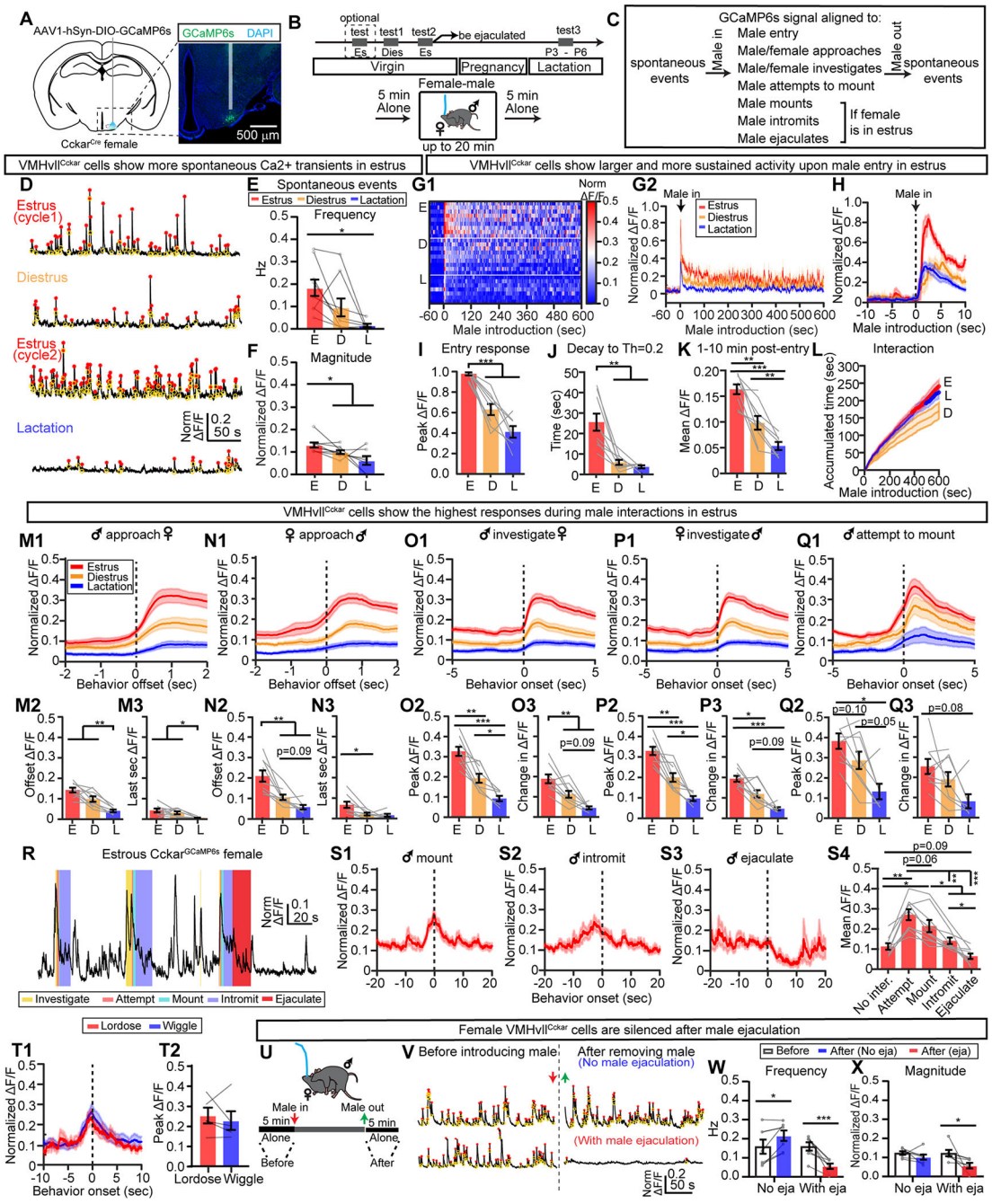

Figure 6. Reproductive-state dependent responses of female VMHvll^{Cckar} cells during male interaction

(A) Fiber photometry recording and histology. Shade indicates optic fiber track.

(B) Recording timeline.

(C) Parameters analyzed in the figure.

(D) Representative traces of Ca^{2+} signal of VMHvll^{Cckar} cells in a solitary females during different reproductive states. Red: transient peaks. Yellow: transient troughs.

(E-F) Frequency (E) and magnitude (F) of spontaneous Ca^{2+} events during estrus diestrus and lactation.

(G) Heatmap of Ca^{2+} traces from individual females (G1) and the average of all females under a specific reproductive state (G2) during male-female interaction. For each animal, signals were normalized to 0–1 by the maximum Ca^{2+} signal across all recording sessions of that animal.
(H) Male entry aligned PETHs of Ca^{2+} signals from all animals under a specified reproductive state.
(I) Peak ΔF/F within the first 60 s after male entry.
(J) The time for the normalized ΔF/F to reach 0.2 after peaking during the male entry.
(K) Mean ΔF/F from 1–10 minutes after male entry.
(L) The accumulated male-female interaction time over 10 minutes when the females were under different reproductive states.
(M1-M3) PETHs of normalized ΔF/F aligned to the offset of male-initiated approach towards the female (M1), value at the offset of approach (M2), change in normalized ΔF/F during the last second of approach (M3).
(N1-N3) Same as (M1-M3) but for female-initiated approach.
(O1-O3) PETHs of normalized ΔF/F aligned to the onset of male investigation of the recording female (O1), Peak ΔF/F during male investigation (O2), and the difference between the peak response and the mean ΔF/F at the preceding baseline (−3 to −1 s) (O3).
(P-Q) Same as (O). Signal aligned to the onset of female investigation of the male (P1-P3) and onset of male mounting attempts (Q1-Q3).
(R) Trace of normalized ΔF/F from an estrous female during copulation. Color shades indicate male behaviors.
(S1-S3) PETHs of normalized ΔF/F aligned to the onset of male mounting (S1), intromission (S2) and ejaculation (S3).
(S4) Mean signal during various male sexual behaviors.
(T1) PETHs of normalized ΔF/F aligned to the onset of female lordosis (red) and wiggling (blue).
(T2) Peak signal during wiggling and lordosis.
(U) The time windows for spontaneous Ca^{2+} transient analysis.
(U) Example traces of Ca^{2+} signals before male introduction (left) and after male removal (right). Top: no ejaculation. Bottom: with ejaculation.
(W and X) Frequency (W) and magnitude (X) of spontaneous Ca^{2+} transients.
Data are mean ± s.e.m. (E, F, I-K, M2-Q2, M3-Q3, S4) One-way ANOVA with repeated measures, followed by Tukey's multiple comparisons test. (L) Two-way ANOVA, followed by Tukey's multiple comparisons test, red and blue dots indicate periods when accumulated time differed significantly ($p<0.05$) between E and D vs. L and D, respectively. (T2) Two-tailed paired t test. (W, X) Two-way ANOVA, followed by Sidak's multiple comparisons test. *p<0.05; **p<0.01; ***p<0.001.
n = number of animals. (D-Q3) n=9 estrous, 9 diestrous and 7 lactating females. (S) n=9 estrous females. (T2) n=5 females. (W-X) n=7 estrous females.
See also Figures S12–S15.

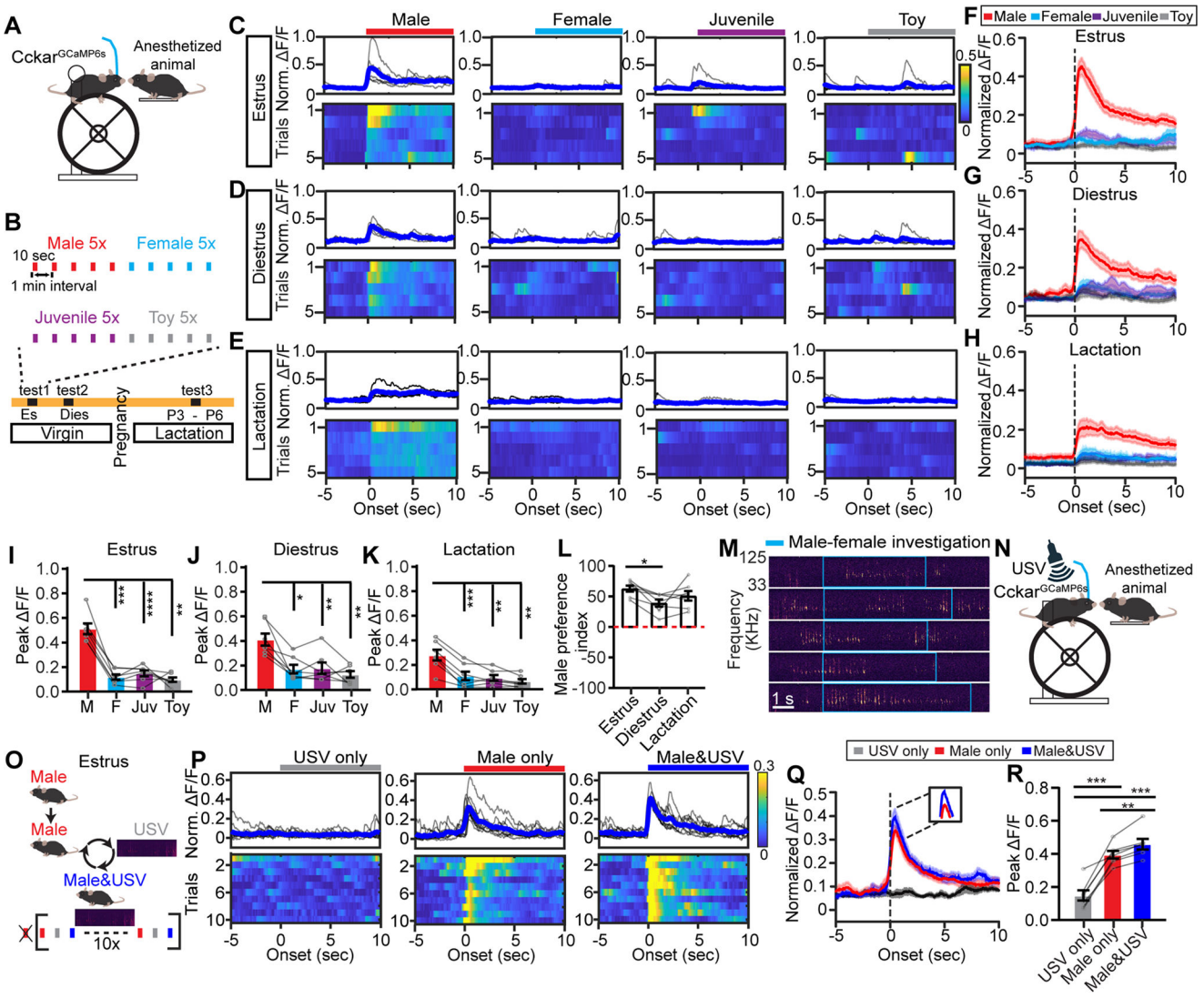

Figure 7. VMHvll^{Cckar} cells preferentially respond to male cues

(A) Head-fixed recording.

(B) Stimulus presentation schedule.

(C-E) Representative PETHs (top) and heatmaps (bottom) of normalized ΔF/F aligned to presentation of an anaesthetized male, female, juvenile, and a toy mouse. Traces are from the same female mouse during estrus(C), diestrus (D) and lactation (E). Blue shows the average.

(F-H) Average PETHs of all animals aligned to the presentation onset of various stimuli when the recording females are in estrus (F), diestrus (G) and lactation (H).

(I-K) Peak ΔF/F during presentation of various stimuli when the recording females are in estrus (I), diestrus (J) and lactation (K).

(L) Male preference index under different reproductive states. Index: (male Peak ΔF/F)/Peak ΔF/F (male + female + juvenile) × 100%.

(M) Representative USV during male investigation of a female (blue box).

(N) Recording schematics to probe VMHvll^{Cckar} cell responses to male USV.

(O) Stimulus presentation schedule.
(P) Representative PETHs (top) and heatmaps (bottom) of normalized ΔF/F aligned to presentation of male USV, an anaesthetized male, and anaesthetized male + USV. Traces from the same estrous female.
(Q) Average PETHs of all animals aligned to the presentation of various stimuli.
(R) Peak responses to various stimuli.
Data are mean ± s.e.m. (I-L, R) One-way ANOVA, followed by Tukey's multiple comparisons test. *p<0.05; **p<0.01; ***p<0.001.
n = number of animals. (F-L, Q-R), n=7 for each group.

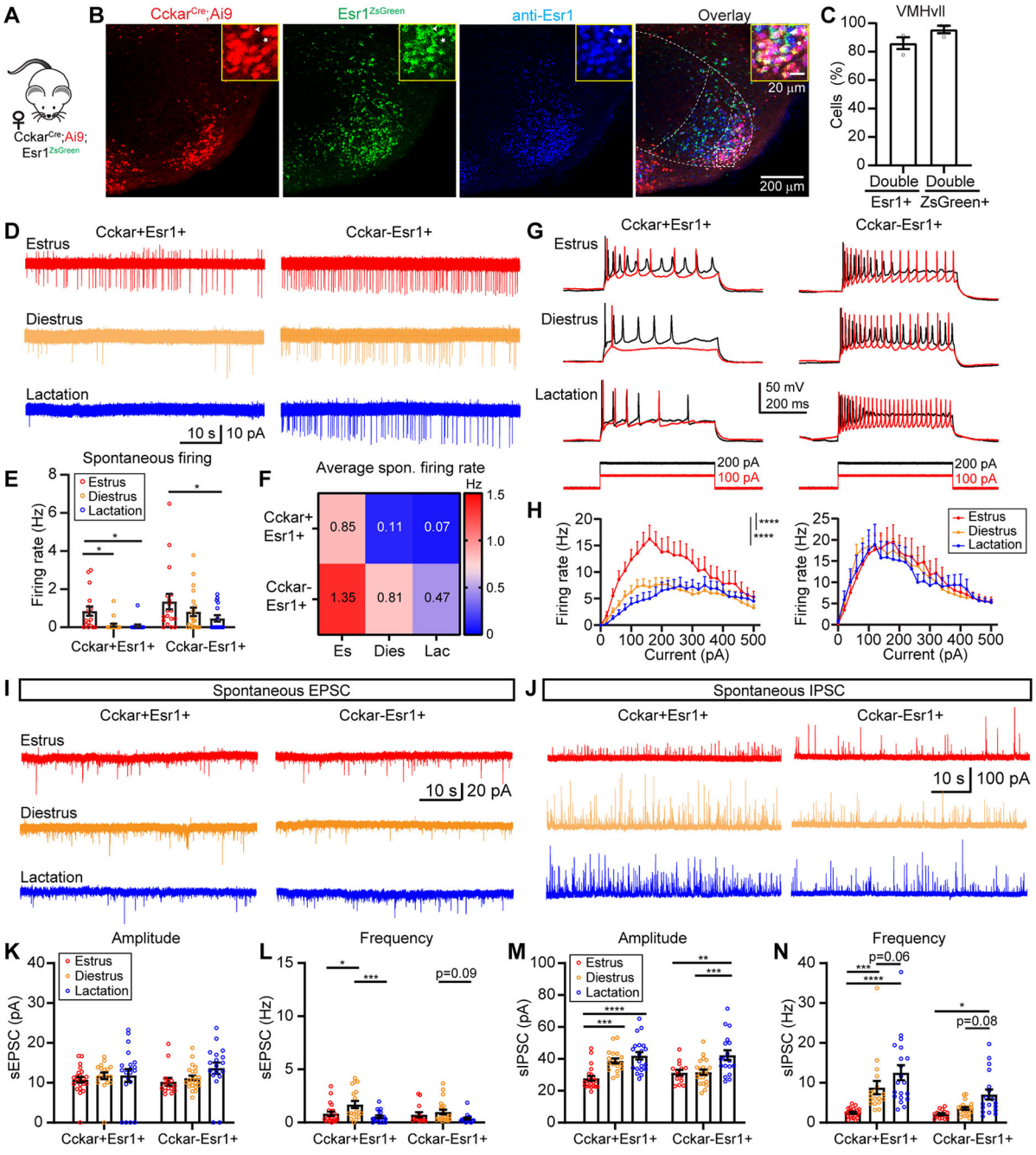

Figure 8. VMHvll^{Cckar} cells change physiological properties over reproductive cycle

(A) Mice used for slice recording.

(B) Left to right showing tdTomato+, Cckar, ZsGreen, anti-Esr1 and overlay of all signals in the VMHvl. Dotted lines demarcate VMH. Inset, magnified region of the boxed area.

(C) Percentage of overlap between Esr1 and ZsGreen.

(D) Representative traces of cell-attached recording of VMHvll$^{Cckar+Esr1+}$ and VMHvll$^{Cckar-Esr1+}$ cells.

(E-F) Bar plots (E) and heatmap (F) showing the spontaneous firing rate under three reproductive states.

(G) Representative recording traces with 100 pA and 200 pA current injections.
(H) F-I curves of female VMHvll$^{Cckar+Esr1+}$ (left) and VMHvll$^{Cckar-Esr1+}$ cells (right).
(I-J) Representative traces of spontaneous EPSCs (I) and IPSCs (J).
(K, L, M, N) Amplitude and frequency of sEPSC (K and L) and sIPSC (M and N).
Data are mean ± s.e.m. (E, H, K-N) Two-way ANOVA followed by Tukey's multiple comparisons test. *p<0.05; **p<0.01; ***p<0.001; ****p<0.0001.
n = number of animals. (C) n=3 animals. (E-H) 17, 19, 16 VMHvll$^{Cckar+Esr1+}$ cells and 18, 22, 16 VMHvll$^{Cckar-Esr1+}$ cells from 3 females of each reproductive state. (K-N) 22, 18, 20 VMHvll$^{Cckar+Esr1+}$ cells and 14, 22, 18 VMHvll$^{Cckar-Esr1+}$ cells from 3 females of each reproductive state.
See also Figure S16.

KEY RESOURCES TABLE

REAGENT or RESOURCE	SOURCE	IDENTIFIER
Antibodies		
guinea pig anti-Fos	Synaptic Systems	Cat. # 226005; RRID:AB_2800522
goat anti-Fos	Santa Cruz Biotechnology	Cat# sc-52-G; RRID:AB 2629503
rabbit anti-Esr1	Millipore	Cat. # 06–935; RRID:AB 310305
goat anti-Guinea pig Cyanine Cy™3	Jackson ImmunoResearch	Cat. # 706–165-148; RRID:AB 2340460
donkey anti-Goat Alexa Fluor 488	Jackson ImmunoResearch	Cat# 705–545-147; RRID:AB 2336933
goat anti-Rabbit Cyanine Cy™5	Jackson ImmunoResearch	Cat. # 711–175-152; RRID:AB 2340607
Bacterial and Virus Strains		
AAV1-hSyn-DIO-hM4Di-mCherry	Addgene; (Krashes et al., 2011)	Addgene# 44362- AAV1
AAV2-hSyn-DIO-hM3Dq-mCherry	Addgene; (Krashes *et al.,* 2011)	Addgene# 44361- AAV2
AAV2-hSyn-DIO-mCherry	Addgene; Bryan Roth lab (unpublished)	Addgene# 50459- AAV2
AAV1-hSyn1-SIO-stGtACR2-FusionRed	Addgene; (Mahn et al., 2018)	Addgene# 105677- AAV1
AAV2-EF1a-DIO-ChR2-EYFP	UNC Vector Core; Karl Deisseroth lab (unpublished)	Cat. # AV-2-AV4378p
AAV2-CAG-Flex-GFP	UNC Vector Core; (Oh et al., 2014)	Cat. # AV-2-ALL854
AAV1-hSyn-Flex-GCaM P6s-WPRE.SV40	Addgene; (Chen et al., 2013)	Addgene# 100843-AAV1
Chemicals, Peptides, and Recombinant Proteins		
Normal donkey serum	Jackson ImmunoResearch	Cat. # 017-000-121; RRID:AB 2337258
Red Retrobeads™	Lumafluor, Inc	N/A
CNO	Sigma	Cat. # 34233-69-7
Critical Commercial Assays		
Nanoliter injector	World Precision Instruments	Cat. # Nanoliter 2000
Temperature Logger	Star-Oddi	DST nano-T
Experimental Models: Organisms/Strains		
$Cckar^{Cre}$ knock-in mice	This Paper	N/A
C57BL/6 mice	Charles River	Strain Code 027
$Esr1^{ZsGreen}$	Yong Yu lab (Saito et al., 2016)	N/A
Ai9 mice	Jackson Laboratory	Strain #007909
Ai6 mice	Jackson Laboratory	Strain #007906
Software and Algorithms		
MATLAB R2019b	MathWorks	https://www.mathworks.com/products/matlab.html; RRID:SCR 001622
Prism 9	GraphPad Software	https://www.graphpad.com/scientific-software/prism/; RRID:SCR 002798
StreamPix 8	NorPix	https://www.norpix.com/products/streampix/streampix.php; RRID:SCR_015773
ImageJ	NIH	https://imagei.nih.gov/ii/index.html; RRID:SCR 003070
pCLAMP 11	Molecular Devices	https://www.moleculardevices.com/; RRID:SCR 011323

REAGENT or RESOURCE	SOURCE	IDENTIFIER
Adobe Photoshop 2020	Adobe	https://www.adobe.com/; RRID:SCR 014199
Adobe Illustrator 2020	Adobe	https://www.adobe.com/; RRID:SCR 010279
Body tracking code	David Anderson lab (Lin et al., 2011)	https://github.com/pdollar/toolbox